

# UC Irvine

## UC Irvine Previously Published Works

### Title

Pre- versus Post-synaptic Forms of LTP in Two Branches of the Same Hippocampal Afferent

### Permalink

<https://escholarship.org/uc/item/6wp6z9n4>

### Journal

Journal of Neuroscience, 44(10)

### ISSN

0270-6474

### Authors

Quintanilla, J

Jia, Y

Pruess, BS

et al.

### Publication Date


2024-03-06

### DOI

10.1523/jneurosci.1449-23.2024

Peer reviewed

# Pre- versus Post-synaptic Forms of LTP in Two Branches of the Same Hippocampal Afferent

J. Quintanilla,<sup>1</sup> Y. Jia,<sup>1</sup> B. S. Pruess,<sup>1</sup> J. Chavez,<sup>1</sup>  C. M. Gall,<sup>1,2</sup> G. Lynch,<sup>1,3</sup> and B. G. Gunn<sup>1</sup>

Departments of <sup>1</sup>Anatomy & Neurobiology, <sup>2</sup>Neurobiology & Behavior, and <sup>3</sup>Psychiatry & Human Behavior, University of California, Irvine, California 92697

There has been considerable controversy about pre- versus postsynaptic expression of memory-related long-term potentiation (LTP), with corresponding disputes about underlying mechanisms. We report here an instance in male mice, in which both types of potentiation are expressed but in separate branches of the same hippocampal afferent. Induction of LTP in the dentate gyrus (DG) branch of the lateral perforant path (LPP) reduces paired-pulse facilitation, is blocked by antagonism of cannabinoid receptor type 1, and is not affected by suppression of postsynaptic actin polymerization. These observations are consistent with presynaptic expression. The opposite pattern of results was obtained in the LPP branch that innervates the distal dendrites of CA3: LTP did not reduce paired-pulse facilitation, was unaffected by the cannabinoid receptor blocker, and required postsynaptic actin filament assembly. Differences in the two LPP termination sites were also noted for frequency facilitation of synaptic responses, an effect that was reproduced in a two-step simulation by small adjustments to vesicle release dynamics. These results indicate that different types of glutamatergic neurons impose different forms of filtering and synaptic plasticity on their afferents. They also suggest that inputs are routed to, and encoded by, different sites within the hippocampus depending upon the pattern of activity arriving over the parent axon.

**Key words:** CA3; endocannabinoid; frequency facilitation; hippocampus; lateral perforant path; long-term potentiation; simulations

## Significance Statement

Within the hippocampus, long-term potentiation (LTP), a substrate for memory encoding, is expressed at pre- and postsynaptic sites in a subfield-specific manner. However, the question of whether the pre- or postsynaptic element determines the location of the potentiated state remains. We have addressed this by taking advantage of the anatomical organization of the lateral perforant path (LPP), which branches to innervate two distinct types of principal cells in dentate gyrus (DG) and field CA3. Results indicate that terminals from the same LPP axons use either pre- or postsynaptic LTP signifying that the target neuron specifies the nature of potentiation. Such target specification allows the hippocampus to route incoming information into two channels that have radically different processing modes.

## Introduction

The entorhinal cortex (EC), via the perforant path, densely innervates both the outer two-thirds of the dentate gyrus (DG) molecular layer and the distal-most apical dendrites (*stratum moleculare*) of field CA3 (Amaral et al., 1990; Amaral, 1993;

Witter, 1993). Given that the sole output of the DG targets CA3, the EC can be seen as having strong direct (monosynaptic) and indirect (disynaptic) routes to the latter region. There has been considerable interest in the functional implications of this arrangement. The direct (EC→CA3) branch will plausibly provide a more reliable representation of cue identity and spatial data conveyed, respectively, by the lateral (LPP) and medial (MPP) segments of the perforant path (Eichenbaum and Fortin, 2005; Hargreaves et al., 2005; Eichenbaum et al., 2012; Hunsaker et al., 2013; Petersen et al., 2013; Reagh and Yassa, 2014), especially in light of the massive convergence of the DG projection to CA3 (Henze et al., 2002; Rollenhagen et al., 2007; Rebola et al., 2017). However, the direct route terminates on the most distal segment of the CA3 apical dendrites and thus at a considerable distance from the spike initiation zone, whereas the DG mossy fiber (MF) axons generate massive, extremely potent terminals located immediately proximal to CA3 cell

Received July 31, 2023; revised Dec. 18, 2023; accepted Jan. 22, 2024.

Author contributions: J.Q., G.L., and B.G.G. designed research; J.Q., Y.J., B.S.P., and J.C. performed research; J.Q., B.S.P., G.L., and B.G.G. analyzed data; J.Q., C.M.G., and B.G.G. edited the paper; J.Q., G.L., and B.G.G. wrote the paper.

This work was supported in part by National Institutes of Health (NIH) National Institute on Drug Abuse (NIDA) Grant #DA047441; NIH NIDA grant #DA044118; NIH National Institute of Child Health and Human Development (NICHD) Grant HD101642; Office of Naval Research Grants N00014-18-1-2114 and N00014-21-1-2940; and the National Science Foundation Graduate Research Fellowship under Grant No. DGE-1839285.

The authors declare no competing financial interests.

Correspondence should be addressed to B. G. Gunn at bggunn16@gmail.com or G. Lynch at g.s.lynch@gmail.com.

<https://doi.org/10.1523/JNEUROSCI.1449-23.2024>

Copyright © 2024 the authors

bodies (Salin et al., 1996; Henze et al., 2002; Nicoll and Schmitz, 2005). A possible interpretation is that the direct route activates discrete populations of CA3 pyramidal cells that provide representations of the cortical information, whereas the indirect (EC→DG→CA3) path elicits a temporally extended response that amplifies and/or promotes encoding of that information (Cox et al., 2019).

Largely missing from the discussion of functional consequences is a consideration of the possibility that the two branches of the perforant path have different physiological properties. Such differences in, for example, long-term potentiation (LTP) or frequency facilitation by LPP→DG versus LPP→CA3 synapses would have profound implications for hypotheses about information flow from the cortex into hippocampus. The likelihood that two synaptic populations formed by the same LPP axons (Tamamaki and Nojyo, 1993; Witter, 1993) are functionally distinct might seem remote, but such effects have been described for same fiber innervation of interneurons versus principle cells in the cerebellum (Bao et al., 2010), hippocampus (Scanziani et al., 1998; Toth et al., 2000; Lawrence and McBain, 2003; Lawrence et al., 2004; Sun et al., 2005; Aldahabi et al., 2022), and neocortex (Reyes et al., 1998; Rozov et al., 2001). If target specification also differs between subtypes of glutamatergic (projection) neurons—a point that has yet to be tested—then the radically different cell types found in the DG versus CA3 might impose very different characteristics on their shared input from LPP axons. We tested this possibility by comparing frequency facilitation, an effect that is firmly linked to transmitter release probability and thus presynaptic mechanisms, at the two LPP termination sites.

The LPP also provides a particularly interesting case for investigating possible regional differences in synaptic plasticity because one of its branches (to DG) has been linked to a presynaptic form of LTP (Wang et al., 2016, 2018b), whereas the other (to CA3) innervates cells that generate a postsynaptic variant of potentiation. While some controversy remains, the preponderance of evidence indicates that LTP in the pyramidal cell→pyramidal cell connection between fields CA3 and CA1 is induced, expressed, and stabilized in the postsynaptic compartment (Kauer et al., 1988; Muller and Lynch, 1988; Nicoll, 2003; Granger and Nicoll, 2014). Much less is known about LTP substrates in DG but recent results indicate that LPP→DG contact uses presynaptic modifications to express and consolidate the potentiated state, although the induction appears to require postsynaptic elements (Chiu and Castillo, 2008; Wang et al., 2016, 2018b). The LPP→CA3 connection thus brings together axons that are clearly capable of expressing LTP with spines that very likely have the same capacity. An analysis of these synapses could therefore provide insights about which element dominates in determining the locus of potentiation. If target cells specify LTP operations, then we would expect to find more conventional CA1 types of plasticity at LPP→CA3 synapses than is the case for LPP→DG connections. The studies reported here tested this prediction.

## Materials and Methods

### Animals

All studies used male C57/BL6 mice (Charles River) from 2 to 4 months of age. Animals were group housed (five per cage) with access to food and water ad libitum and were on a 12 h light/dark cycle, with lights on at 6:30 A.M. Experiments were conducted in accordance with the Institutional Animal Care and Use Committee at the University of California, Irvine and the National Institute of Health Guidelines for the Care and Use of Laboratory Animals. For all electrophysiology studies, mice were anesthetized with isoflurane and killed by decapitation.

### Extracellular hippocampal field recordings

Hippocampal slices were prepared as previously described (Cox et al., 2019; Quintanilla et al., 2022). Experiments were initiated from 8 to 10 A.M. Upon removal from the cranium, brains were placed in ice-cold, oxygenated (95% O<sub>2</sub>/5% CO<sub>2</sub>) high Mg<sup>2+</sup>, artificial cerebrospinal fluid (HM-aCSF) containing the following (in mM): 87 NaCl, 26 NaHCO<sub>3</sub>, 25 dextrose, 75 sucrose, 2.5 KCl, 1.25 NaH<sub>2</sub>PO<sub>4</sub>, 0.5 CaCl<sub>2</sub>, 7 MgCl<sub>2</sub> (320–335 mOsm). Horizontal sections were cut at a thickness of 360 μm using a Leica Vibratome (model VT1000s) into cold HM-aCSF and rapidly transferred to an interface recording chamber containing a constant perfusion (60–70 ml/h) of oxygenated (95% O<sub>2</sub>/5% CO<sub>2</sub>) aCSF containing the following (in mM): 124 NaCl, 3 KCl, 1.25 KH<sub>2</sub>PO<sub>4</sub>, 1.5 MgSO<sub>4</sub>, 26 NaHCO<sub>3</sub>, 2.5 CaCl<sub>2</sub>, and 10 dextrose, pH 7.4 (300–310 mOsm, 31 ± 1°C). Recordings began 1.5–2 h later. For all hippocampal field studies, recordings were digitized at 20 kHz using an AC amplifier (A-M Systems, model 1700) and collected using NacGather 2.0 (Theta Burst Corp.).

For field recordings of LPP-evoked responses, a stimulating (twisted nichrome wire) electrode was placed in the outer third of the DG molecular layer at the edge of the internal blade and a recording electrode was positioned either in *stratum (str.) moleculare* of field CA3 or in the outer third of the DG molecular layer. In both cases, paired-pulse stimulation (40 ms interpulse interval) was used to verify a positive paired-pulse ratio (PPR); that is, the initial slope of the second response expressed as a percent of that of the first, as is characteristic of the LPP and which distinguishes this system from the MPP (McNaughton, 1980; Christie and Abraham, 1994; Berzhanskaya et al., 1998). Single-pulse baseline stimulation was applied at 0.05 Hz, with intensity set at ~50% of the maximum population-spike free field excitatory postsynaptic potential (fEPSP). A subset of experiments investigated if LPP axons terminating in CA3 *str. moleculare* may also form synapses in the outer third of the molecular layer onto granule cells. To test this, we positioned a stimulating electrode in the LPP→CA3 terminal field (as above) and recorded responses to antidromic stimulation from a pipette placed in the outer third of the DG molecular layer (Fig. 1A). An input–output (I/O) curve was generated before recording a sampling period (40 min) of single-pulse antidromic stimulation (0.05 Hz), which was followed by stimulation with a brief (10-pulse) 50 Hz train. This was repeated in slices where a single knife cut was used to sever the LPP (Fig. 1A).

For studies of LTP, baseline responses were recorded for 20 min after which LTP was induced. For LPP→CA3 and LPP→DG synapses, LTP was induced using either two trains of theta burst stimulation (TBS) or high-frequency stimulation (HFS). For induction using TBS, each train (10 bursts of four pulses at 100 Hz with 200 ms between bursts) was separated by 30 s with pulse duration doubled relative to baseline stimulation. HFS induction consisted of a single 1 s, 100 Hz train with pulse duration doubled and intensity increased by ×1.5 relative to baseline stimulation. For both regions and methods of LTP induction, recordings of responses to baseline stimulation resumed for 60 min. In a subset of experiments, LPP→CA3 LTP was induced in slices where the MF projection (DG→CA3) was severed using a single knife cut between the external and internal blade of the DG (Fig. 1A). To confirm the MF cut, we placed a stimulating electrode in the hilus proximal to the granule cell layer at the apex of the two blades of the DG. A recording pipette was then placed in the pyramidal cell layer of CA3b and responses to a 20 Hz train recorded. For studies evaluating the degree of PPF before and after LTP, five paired stimuli (40 or 120 ms interpulse interval; 5 min between pairs) were given during the 20 min baseline period and a second set of five paired pulses were given 60 min after LTP induction. To evaluate short-term plasticity, we recorded responses to 10 pulse trains at 5 Hz, 20 Hz, and 50 Hz. Trains at the different frequencies were delivered in randomized order and spaced by at least 10 min of stable baseline recording. In separate cases, identical stimulation trains were applied to slices in which MF projections were cut (as above).

**Pharmacological treatments.** A subset of experiments tested the role of endocannabinoid signaling at the LPP→CA3 and LPP→DG synapses. Following a period of stable baseline recording (20 min), the cannabinoid type 1 receptor (CB1R) inverse agonist AM251 (5 μM) was applied

to the chamber via a second infusion line (6 ml/h) for 40 min prior to LTP induction with TBS (as above). A second set of experiments tested the effect that 1 h infusion of the CB1R agonist, WIN55-212-2 (WIN; 5  $\mu$ M) had upon baseline transmission. A separate set of experiments used the phorbol ester, phorbol 12,13-di-butylate (PDBU; 1  $\mu$ M), to test how increasing release probability influenced responses to repetitive stimulation. Responses to 50 Hz LPP stimulation (10 pulses) were recorded at LPP→DG and LPP→CA3 synapses prior to, and following, a 40 min infusion of PDBU.

All extracellular recordings were analyzed offline using NACShow 2.0 (Theta Burst Corp.). For LTP experiments, the fEPSPs rising slopes (20–80%) were measured across the entire recording and then normalized to a 20 min baseline period. The magnitude of LTP was determined by comparing the mean slope of fEPSPs collected during the last 5 min of baseline recordings with the mean response for last 5 min of the recording (i.e., 55–60 min after LTP induction). The fEPSP decay  $\tau$  was described using a monoexponential equation ( $Y(t) = A \cdot \exp(-t/\tau)$ ) and measured across the last 5 min of baseline period and the last 5 min of recording (i.e., 55–60 min). The fEPSP waveform evoked by paired-pulse stimulation (40 ms and 120 ms intervals) was analyzed with regard to rising slope and decay  $\tau$ . The effect of pharmacological treatment (e.g., AM251, WIN) were assessed upon the baseline fEPSP waveform, which was analyzed with regard to peak amplitude, rising slope (20–80%), and decay  $\tau$ , before any effects upon paired-pulse stimulation and/or LTP were assessed (as above). Responses to stimulation at set frequencies (i.e., 5 Hz, 20 Hz and 50 Hz) were analyzed with regard to the fEPSP rising slope (20–80%) or the amplitude of the waveform. The fEPSP slopes or amplitudes were measured across the stimulation train and then normalized to the first response (% pulse 1). For drug treatment studies (e.g., PDBU), measures of fEPSP slopes in response to 50 Hz stimulation, in the absence and presence of the specific compound, were normalized as described above.

#### Whole-cell recordings

For whole-cell patch-clamp experiments, hippocampal slices were prepared as previously described (Gunn et al., 2017). Briefly, the brain was rapidly removed and placed in ice-cold oxygenated (95% O<sub>2</sub>–5% CO<sub>2</sub>) aCSF containing the following (in mM): 124 NaCl, 3 KCl, 1.25 KH<sub>2</sub>PO<sub>4</sub>, 3 MgSO<sub>4</sub>, 26 NaHCO<sub>3</sub>, and 10 dextrose, pH 7.4 (300–310 mOsm). Horizontal slices were cut (370  $\mu$ m) using a Leica Vibratome at 4°C and then transferred to a holding chamber where they were incubated at room temperature for at least 1 h in oxygenated aCSF containing the following (in mM): 124 NaCl, 3 KCl, 1.25 KH<sub>2</sub>PO<sub>4</sub>, 1.5 MgSO<sub>4</sub>, 26 NaHCO<sub>3</sub>, 2.5 CaCl<sub>2</sub>, and 10 dextrose, pH 7.4 (300–310 mOsm). Slices were then transferred to the recording chamber and continuously perfused in the same oxygenated aCSF maintained at 30 ± 1°C.

A small-diameter (1  $\mu$ m) bipolar stimulating electrode (World Precision Instruments) placed in the CA3 *str. moleculare* was used to evoke LPP-specific excitatory postsynaptic currents (eEPSC). LPP→eEPSCs were recorded from visually identified CA3 pyramidal cells at a holding potential of –70 mV in aCSF that additionally contained PTX (50  $\mu$ M). Patch pipettes (5–8 M $\Omega$ ) were pulled from thick-walled borosilicate glass (1.5 mm outer diameter; 0.86 mm inner diameter; Sutter Instrument) and filled with an internal solution containing the following (in mM): 130 CsCH<sub>3</sub>SO<sub>4</sub>, 8 CsCl, 8 NaCl, 10 HEPES, 0.2 EGTA, 2 Mg-ATP, 0.3 Na-GTP, 2 QX-314 (Sigma-Aldrich). Alexa Fluor 594 (0.3  $\mu$ M; Thermo Fisher Scientific) was additionally included in the internal solution to enable visualization of the recorded cell's dendrites and confirm proximity of the stimulating electrode. Paired-pulse stimulation (40 ms) was used to confirm activation of LPP→CA3 synapses (McNaughton, 1980; Christie and Abraham, 1994; Berzhanskaya et al., 1998). Single-pulse baseline stimulation was applied at 0.05 Hz (i.e., every 20 s). Baseline eEPSCs were recorded for 5 min before applying two 10 burst trains of TBS [holding at 0 mV], separated by 30 s, to induce LTP. In a subset of experiments, latrunculin A (Lat-A; 400 nM) was included in the recording pipette to determine if postsynaptic actin polymerization was required for LTP at the LPP→CA3 synapse. Currents were filtered at 2 kHz using an eight-pole Bessel filter. Only those cells with a stable access resistance were used, with recordings being aborted if >20% change in series resistance occurred. All

recordings were made using an Axopatch 200A (Molecular Devices) and pClamp 10. Recordings were stored directly to a PC (4 kHz digitization) using a Digidata 1550A (Molecular Devices).

All recordings were analyzed offline using the Strathclyde Electrophysiology Software (WinEDR and WinWCP; Dr. J. Dempster, University of Strathclyde). Individual eEPSCs were detected in WinEDR using a method based on a rate of rise threshold that targeted the stimulation artifact and was specific for individual cells. Detected events were visually inspected, and any traces containing noise or multiple synaptic responses were removed from the analysis. Accepted events were analyzed with regard to peak amplitude. Ensemble average eEPSCs (minimum of 10 events) were generated for each cell before and following expression of stable LTP. Averaged synaptic currents were analyzed with regard to their decay  $\tau$ , which was best described by the single exponential function  $Y(t) = Ae^{-t/\tau}$ . The eEPSCs in response to paired-pulse stimulation (40 ms interval) were analyzed with regard to peak amplitude and then normalized to the amplitude of the first response (i.e., P2/P1). The magnitude of LTP was determined by comparing the peak amplitude of eEPSCs collected during the 5 min pre-LTP baseline period with those obtained during the last 5 min of the recording (i.e., 45–50 min after LTP induction).

#### Drug application

Compounds used in hippocampal slice experiments were introduced to the bath via a second, independent perfusion line (6 ml/h). AM251 (50 mM), WIN (50 mM), and PDBU (10 mM) were prepared as stock solutions in dimethyl sulfoxide (DMSO). Each was then diluted in aCSF to achieve the desired final concentration (AM251, 5  $\mu$ M; WIN, 5  $\mu$ M; PDBU, 1  $\mu$ M), with  $\leq 0.01\%$  DMSO in aCSF bath. For whole-cell recordings, PTX was made as a stock solution (50 mM) in DMSO and diluted to the final concentration (50  $\mu$ M) in aCSF. Lat-A (400 nM) was made directly in the electrode internal solution. All compounds were obtained from Tocris.

#### Monte Carlo simulations of a two-step release model

To test if factors within the presynaptic terminal may be critical determinants of the short-term operations occurring at the LPP→CA3 synapse, we used a previously published (Miki et al., 2016; Quintanilla et al., 2022) renewable two-step release model based upon Monte Carlo simulations using Igor Pro (WaveMetrics). Briefly, the two-step release model incorporates four factors associated with the release and subsequent replenishment of synaptic vesicles. These include the probability of docking site occupancy ( $\delta$ ) and the probability of docked vesicle release ( $p_v$ ). The product of these two factors (i.e.,  $\delta p_v$ ) describes the overall probability of release ( $p$ ). Each synapse has a number of docking sites ( $N$ ) that are supplied from a pool of replacement vesicles. The movement of replacement vesicles to empty docking sites is described by the probability “ $r$ ”. The replacement vesicle pool has an occupancy probability of 1 prior to stimulation, with replenishment of this replacement pool occurring with a probability “ $s$ ” following replacement vesicle depletion associated with repetitive activation.

Our previous studies, using a modified version of the original common replacement pool model (Miki et al., 2016), conducted a parameter search to identify the combination of variables that most reliably recapitulated the experimental data recorded from the LPP→DG synapse following 50 Hz (10 pulses) stimulation (Quintanilla et al., 2022). The optimized parameters for the LPP→DG terminals are as follows:  $\delta = 0.6$ ;  $p_v = 0.55$ ;  $r = 0.7$ ;  $s = 0.4$ ;  $N = 3$ ; pool size, 3 vesicles. To identify factors involved in vesicle release that may potentially differ between the two LPP branches, simulations used variants of the above parameters (Quintanilla et al., 2022) based upon the electrophysiological differences identified at the two terminals. These differences were almost entirely associated with  $p$ , and as such in the majority of simulations only the variables directly associated with this,  $\delta$  and  $p_v$ , were modified (unless otherwise stated). As in previous studies, the variables within the model were constrained to generate this optimized set of parameters as follows:  $\delta > 0.2$  and  $< 0.8$ ;  $p_v > 0.2$  and  $< 0.8$ ;  $r > 0.2$  and  $< 0.8$ ; and  $s > 0.2$  and  $< 0.8$ . Values for  $\delta$  and  $p_v$  were separated by a probability of  $< 0.1$  (unless stated). The simulation was repeated 50 times with each combination of variables

to an accuracy of 0.05 probability. The simulated output (i.e., vesicle number) was normalized to the initial response (i.e., pulse 1) and then fit to the normalized LPP→CA3 curves generated from the electrophysiological data. The standard error between each individual point (i.e., pulse number) was compared and a mean value generated. Under such conditions, a parameter space was then computed using a modified version of the original code (Miki et al., 2016) generated using Python 3.8.

**The effect of reducing  $p$ .** Initial experiments tested if reducing only  $p$  in the optimized LPP→DG synapse (above) could recapitulate the output profile recorded from the LPP→CA3 synapse. The initial  $p$  (i.e.,  $\delta p_v$ ) of 0.33 was incrementally decreased (0.25, 0.20, and 0.16) and the effects upon the output profile determined. When reducing  $p$ , the relative contribution of  $\delta$  and  $p_v$  were equal (0.25:  $\delta=0.5$ ,  $p_v=0.5$ ; 0.20:  $\delta=0.45$ ,  $p_v=0.45$ ; 0.20:  $\delta=0.4$ ,  $p_v=0.4$ ). A parameter search, using the modified code, was conducted to identify the optimal value for  $p$  (i.e., combination of  $\delta$  and  $p_v$ ) to most reliably reproduce the electrophysiological data recorded from the intact and MF cut slices when all other parameters were unchanged.

**Selectively reducing the individual components of release:  $\delta$  and  $p_v$ .** To test the contribution that  $\delta$  and  $p_v$  make to the simulated output curve, we ran the model in two different configurations that produced the same overall  $p$  of 0.22. To do this, we unconstrained the model such that  $\delta$  and  $p_v$  could be separated by a probability of  $>0.1$ . In the first configuration,  $\delta=0.4$  and  $p_v=0.55$ , while the values for these parameters in the second version were reversed (i.e.,  $\delta=0.55$  and  $p_v=0.4$ ). The simulated output curve following 50 Hz stimulation was generated for each configuration of the model. In a second set of simulations, a parameter search was conducted to identify the optimal vesicle recycling parameters (i.e.,  $r$  and  $s$ ) to reproduce the 50 Hz LPP→CA3 curve when only  $\delta$  was reduced.

**The effect of increasing  $p$  with PDBU.** To test how a PDBU-induced increase in vesicular release may influence the output curve to 50 Hz activation, at the optimized LPP→DG and LPP→CA3 synapses, we ran the model under conditions where the two parameters associated with release probability (i.e.,  $\delta$  and  $p_v$ ), were increased by a factor of 0.2.

The simulated output curves and the potential differences predicted for each synapse could then be tested empirically.

### Statistical analysis

All results are presented as group means  $\pm$  SEM. Statistical comparisons of PPF and LTP used either paired or unpaired Student's  $t$  tests (GraphPad Prism version 6.0), unless otherwise stated in text or figure legends. For all studies, the group  $N$  refers to the number of slices for extracellular field recordings or cells for whole-cell recordings, with a minimum of three animals per group. Additional specific statistical tests,  $N$  values, and degrees of freedom are presented within the figure legends. For all studies,  $p$  values of  $<0.05$  were considered significant.

## Results

### Induction of LTP in LPP projections to CA3 does not influence the PPR

Single-pulse stimulation delivered to the DG outer molecular layer near the junction with CA3 elicited a large fEPSP in *str. moleculare* of the latter region (Fig. 1A). This was accompanied by a positive going potential in the CA3 cell body layer. We next looked to confirm findings from anatomical studies that indicate LPP projections terminating within the outer molecular layer of the DG also extend to innervate the distal apical dendrites of CA3 pyramidal cells (Tamamaki and Nojyo, 1993; Witter, 1993). To test this, we stimulated the LPP terminal zone in CA3 *str. moleculare* and recorded the antidromically evoked response in the outer molecular layer of the medial DG (Fig. 1A,B). The fEPSPs elicited in the DG by antidromic LPP stimulation displayed the expected input–output relationship (Fig. 1B) and were stable in response to single-pulse stimulation over a prolonged (40 min) baseline period (Fig. 1C). A brief 50 Hz train (10 pulses) of antidromic stimulation produced a biphasic output profile that was similar to that observed following orthodromic LPP→DG stimulation (pulse 10; antidromic,

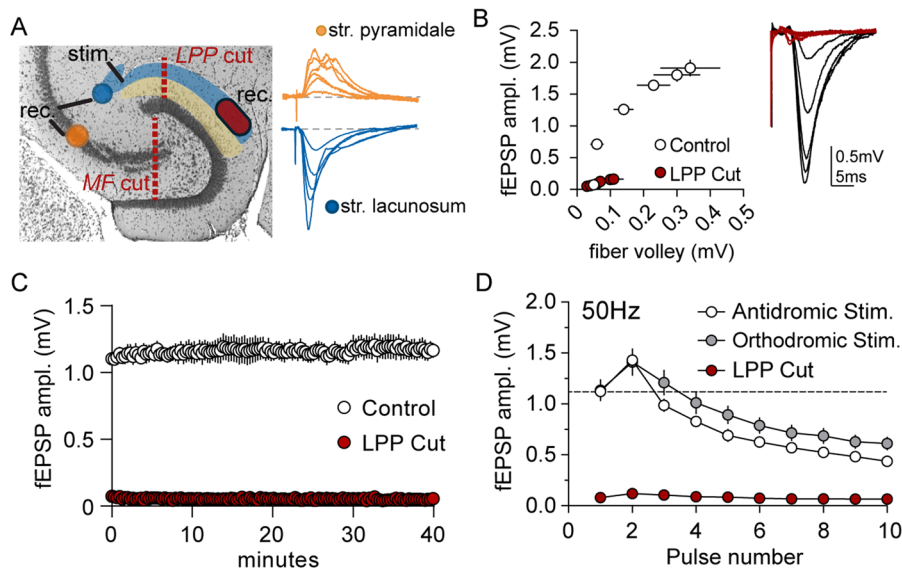


**Figure 1.** A significant proportion of LPP axons innervate both CA3 pyramidal cells and DG granule cells. **A**, Nissl-stained hippocampal slice (left) illustrating the arrangement of the stimulating electrode and recording pipettes to record (1) responses in CA3 str. pyramidale (orange) and str. moleculare (blue) following orthodromic LPP stimulation and (2) responses from the outer molecular layer of medial DG (red) elicited by antidromic LPP activation. The location of the knife cuts to the LPP and MF are illustrated (red dashed line). Representative LPP-evoked fEPSP responses (right) recorded from str. pyramidale (orange) and str. lacunosum (blue) of CA3 across a range of stimulation intensities. **B**, Graph summarizing the input–output relationship of responses recorded from the DG following antidromic LPP stimulation in the intact slice (white) and following a single cut to the LPP projection (red). Representative traces are illustrated (right). Scale bars:  $y=0.5$  mV;  $x=5$  ms. **C**, Graph summarizing the amplitude of single-pulse baseline responses elicited by antidromic LPP stimulation in the intact (white) and LPP cut (red) slices. **D**, Graph summarizing the output profile of DG responses elicited by orthodromic (gray) and antidromic (white) 50 Hz stimulation without cut (pulse 10: orthodromic,  $0.61 \pm 0.07$  mV; antidromic,  $0.44 \pm 0.05$  mV;  $p=0.10$ ; Tukey's post hoc test) and antidromic stimulation with LPP cut (red).

$0.44 \pm 0.05$  mV; orthodromic,  $0.61 \pm 0.07$  mV;  $p = 0.10$ ; Tukey's post hoc test; Fig. 1D). LPP→DG responses evoked by single-pulse and repetitive antidromic stimulation were almost completely ablated following the introduction of a knife cut through the LPP between the stimulation and recording sites (Fig. 1A–D). These data indicate that at least a significant proportion of LPP projections terminating in field CA3 also innervate the DG granule cells.

Two trains of TBS produced a robust LTP in LPP→CA3 synapses but not in LPP→DG contacts (LPP→CA3,  $144.8 \pm 4.6\%$  potentiation; LPP→DG,  $110.3 \pm 5.3\%$  potentiation; two-way ANOVA interaction,  $p = 0.036$ ; Tukey's post hoc;  $p = 0.004$ ; Fig. 2A,C). The 1 s trains of HFS (100 Hz) commonly used, and verified here, to induce LTP in the DG also produced robust LTP in the LPP→CA3 connections (LPP→CA3,  $157.6 \pm 12.2\%$  potentiation; LPP→DG,  $154.7 \pm 8.9\%$  potentiation; Tukey's post hoc;  $p = 0.99$ ; Fig. 2B,C). Thus, LPP→DG synapses only reliably produced stable LTP with HFS, whereas LPP→CA3 synapses did so with both TBS and HFS (Fig. 2C). There was however a distinct difference in the potentiation produced by the two induction patterns at the LPP→CA3 synapse: TBS broadened the fEPSP while HFS did not. The mean decay  $\tau$  values for responses during the last 5 min of baseline versus 55–60 min after LTP induction were tightly correlated for both TBS ( $r = 0.8957$ ) and HFS ( $r = 0.8653$ ) but there was a substantial LTP-associated increase in the former case but not the latter (TBS,  $45.2 \pm 8.6\%$ ;  $p = 0.00018$ ; HFS,  $0.41 \pm 4.36\%$ ;  $p = 0.98$ ; Fig. 2D). The difference between the two groups in percent change following LTP induction was highly significant ( $p = 0.0013$ ; unpaired  $t$  test). LTP in the LPP→DG connections did not measurably affect the waveform

of the fEPSP (TBS,  $15.23 \pm 6.80\%$ ;  $p = 0.08$ ; HFS,  $8.89 \pm 5.8\%$ ;  $p = 0.62$ , Fig. 2E). It is not clear why TBS affected the waveform of the evoked response—electron microscopic studies have not uncovered any evident differences in boutons in the *str. moleculare* relative to *str. radiatum* nor any of the peculiarities found in MF connections with CA3 pyramidal cells (Matsuda et al., 2004).

Measures of the PPR provide a simple test of whether a given manipulation enhances synaptic responses by increasing evoked transmitter release (Del Castillo and Katz, 1954; Jackman and Regehr, 2017). Original tests for such effects in CA3→CA1 projections proved negative: robust LTP did not measurably alter the PPR (Muller and Lynch, 1989). This, together with other lines of evidence, led to the conclusion that for field CA1, the stable expression of potentiation was due to postsynaptic modifications (Kim and Lisman, 1999; Krucker et al., 2000; Kramar et al., 2006; Chen et al., 2007; Lauterborn et al., 2017). In contrast, more recent work showed that LTP in the LPP→DG connection is accompanied by a marked reduction in the PPR, as expected for a presynaptic variant of potentiation and specifically with increased transmitter release by potentiated synapses (Wang et al., 2016, 2018b). Before performing a comparable analysis on the CA3 branch of the LPP, we ran tests of whether the first response alters the waveform of the second within a pair. If interactions were to be present in PPR tests, then an effect of LTP on these interactions could be mistaken for an action on release kinetics, an issue that is of particular importance when, as in the present case, potentiation alters the waveform of a first response.

With paired-pulse stimulation of LPP→CA3 synapses, the decay  $\tau$  of the second response was accelerated relative to that

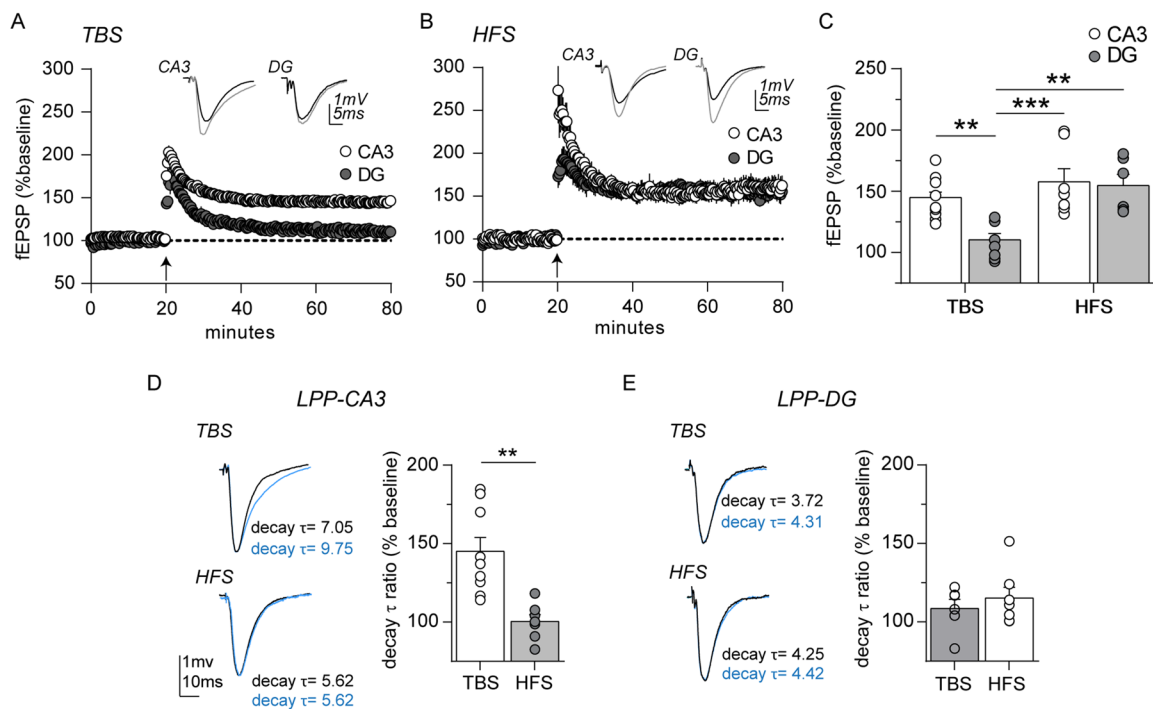


**Figure 2.** LTP induced by TBS or HFS differs between LPP→CA3 and LPP→DG synapses. **A**, Using TBS (at arrow), LTP was induced and persisted in LPP→CA3 synapses but potentiation failed to stabilize in LPP→DG synapses. Representative traces show evoked responses before (black) and 60 min after (gray) TBS for both regions (CA3,  $n = 12$ ; DG,  $n = 8$ ). **B**, Both regions exhibited robust LTP with the HFS induction paradigm. Representative traces show evoked responses before (black) and 60 min after (gray) HFS for both regions (CA3,  $n = 8$ ; DG,  $n = 6$ ). **C**, The magnitude of TBS and HFS-induced LTP, as assessed 55–60 min following induction, shows a failure to express stable LTP at LPP→DG synapses with TBS ( $F_{(1,29)} = 4.80$ ;  $p = 0.036$ ; two-way ANOVA interaction; Tukey's post hoc:  $**p < 0.01$ ,  $***p < 0.001$ ). **D**, Left, Normalized representative traces recorded from LPP→CA3 before (black) and 60 min after (blue) LTP induction with TBS and HFS. Note the clear prolongation of the fEPSP decay tau ( $\tau$ ) with TBS-induced LTP. Right, Graph summarizing the effect of TBS- and HFS-induced LTP on the decay  $\tau$  of fEPSPs (TBS,  $n = 11$ ; HFS,  $n = 7$ ;  $**p < 0.0013$ , unpaired Student's  $t$  test). **E**, Left, Normalized representative traces recorded from LPP→DG before (black) and 60 min after (blue) LTP induction with TBS and HFS. Right, TBS and HFS LTP had no effect on the LPP→DG decay  $\tau$  (TBS,  $n = 7$ ; HFS,  $n = 6$ ;  $p = 0.48$ ).

of the first when the paired pulses were separated by 40 ms (CA3:  $P_1 = 5.17 \pm 0.36$  ms,  $P_2 = 3.47 \pm 0.15$  ms;  $n = 8$ ,  $t_{(7)} = 4.38$ ,  $p = 0.003$ ; Fig. 3A,B). This was not the case for an interpulse interval of 120 ms ( $P_1 = 5.02 \pm 0.35$  ms,  $P_2 = 5.0 \pm 0.35$  ms;  $n = 10$ ,  $t_{(9)} = 0.55$ ,  $p = 0.592$ ; Fig. 3A,B). As expected, the first response affects the shape of the second only when the two occur in rapid succession. We accordingly tested for an effect of TBS-induced LTP on the PPR in CA3 using a 120 ms interpulse interval. The mean PPR measured in the last 5 min of baseline ( $64.7 \pm 4.2\%$ ) was not significantly different from that recorded 55–60 min after TBS ( $62.4 \pm 4.6\%$ ;  $n = 8$ ;  $p = 0.07$ ; paired  $t$  test; Fig. 3C). HFS-induced CA3 LTP, which does not affect the waveform of the fEPSP, also had no effect on the PPR when pulses were separated by 120 ms (baseline,  $72.5 \pm 2.9\%$ ; 60 min post-HFS,  $71.9 \pm 2.3\%$ ;  $n = 5$ ;  $p = 0.65$ ; Fig. 3C). Finally, HFS-induced potentiation had little if any effect on PPR when tested with pulses separated by 40 ms ( $104.7 \pm 2.0\%$  vs  $99.7 \pm 3.5\%$ ;  $n = 7$ ;  $p = 0.06$ ).

There were no detectable decay  $\tau$  differences between paired-pulse responses 1 and 2 in the LPP→DG projection for interpulse intervals of 40 ms (DG:  $P_1 = 3.24 \pm 0.37$  ms,  $P_2 = 3.39 \pm 0.31$  ms;  $n = 10$ ,  $t_{(9)} = 0.58$ ,  $p = 0.582$ ) or 120 ms ( $P_1 = 3.96 \pm 0.31$  ms,  $P_2 = 3.68 \pm 0.37$  ms;  $n = 8$ ,  $t_{(7)} = 1.72$ ,  $p = 0.130$ ; Fig. 3D,E). In contrast to the CA3 results, induction of LTP in the DG branch of the LPP produced a significant reduction in the PPR when pulses were separated by 120 s (baseline,  $40.7 \pm 4.2\%$  to  $31.2 \pm 4.4\%$ ;  $n = 8$ ;  $p = 0.003$ ) or, as in earlier reports (Wang et al., 2018b),

by 40 ms ( $58.4 \pm 3.8$  to  $45.5 \pm 3.8$ ;  $n = 6$ ;  $p = 0.004$ ; Fig. 3F). The percent change in PPR was not reliably different for the two intervals (40 ms,  $-20.3 \pm 4.3\%$ ; 120 ms,  $-19.0 \pm 4.3\%$ ;  $p = 0.83$ ).

We conclude from these results that LTP in the CA3 branch of the LPP does not cause a significant change in PPR and accordingly is not likely due to an increase in transmitter release. This result stands in contrast to the decrease in PPR associated with potentiation of LPP→DG synapses.

### LPP→CA3 potentiation is not CB1R dependent

LTP in the DG branch of the LPP is markedly reduced with CB1R knock-out or pharmacological suppression (Wang et al., 2016, 2018a,b; Piette et al., 2020) and multiple lines of evidence established that 2-arachidonylglycerol (2-AG) is the endocannabinoid used by LPP→DG synapses to elicit enduring LTP at this terminal. As 2-AG is synthesized postsynaptically and CB1Rs are localized to LPP terminals (Katona et al., 2006; Kano et al., 2009; Castillo et al., 2012; Wang et al., 2016), these results indicated that potentiation is initiated in spines and expressed presynaptically by an increase in neurotransmitter release (Wang et al., 2016, 2018b). This accords with the above described depression of the PPR in LPP→DG synapses following induction of LTP (Christie and Abraham, 1994; Wang et al., 2016). In contrast to these results, the selective CB1R inverse agonist AM251 (5  $\mu$ M) had no evident effect on LTP in LPP→CA3 synapses. The percent potentiation measured 55–60 min postinduction was  $50.5 \pm 4.1\%$  and

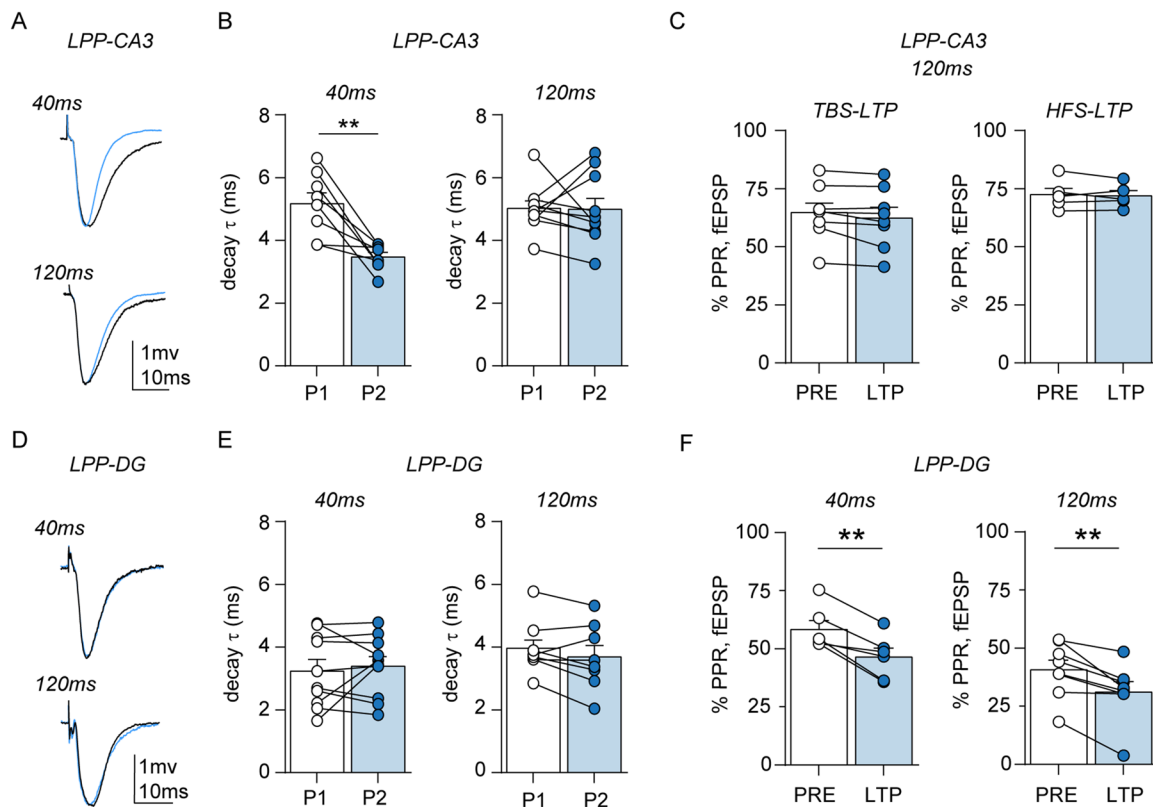


**Figure 3.** LTP alters the PPR at LPP→DG but not LPP→CA3 synapses. Responses to paired-pulse stimulation (PPS) were assessed for LPP→CA3 (A–C) and LPP→DG (D–F) synapses. **A**, Superimposed and normalized first (black) and second (blue) LPP→CA3 fEPSP responses to PPS using 40 ms and 120 ms interpulse intervals. **B**, Graphs summarizing the mean decay  $\tau$  of responses to the first (P1) and second (P2) LPP→CA3 response show a P1 to P2 reduction for the 40 ms interpulse interval only (40 ms:  $n = 8$ ,  $t_{(7)} = 4.38$ ,  $**p = 0.003$ ; 120 ms:  $n = 10$ ,  $t_{(9)} = 0.55$ ,  $p = 0.592$ ; paired Student's  $t$  test). **C**, There were no changes in the LPP→CA3 PPR from before and to 60 min after LTP induction, using either TBS ( $n = 8$ ;  $t_{(7)} = 2.17$ ;  $p = 0.07$ ) or HFS ( $n = 5$ ;  $t_{(4)} = 0.49$ ;  $p = 0.65$ ), when pulses were separated by 120 ms. **D**, Superimposed normalized first (black) and second (blue) responses recorded from LPP→DG following PPS with 40 ms and 120 ms interpulse intervals. **E**, LPP→DG synapses exhibited no P1 to P2 difference in the mean decay  $\tau$  with PPS interpulse intervals of 40 ( $n = 10$ ;  $t_{(9)} = 0.57$ ;  $p = 0.58$ ) or 120 ms ( $n = 8$ ;  $t_{(7)} = 1.72$ ;  $p = 0.13$ ). **F**, Bar graphs show that following the induction of LPP→DG LTP, the PPR is reduced with 40 and 120 ms intervals (40 ms:  $n = 6$ ,  $t_{(5)} = 4.99$ ,  $**p = 0.004$ ; 120 ms:  $n = 8$ ,  $t_{(7)} = 4.39$ ,  $**p = 0.003$ ).

47.9 ± 3.8% for slices treated with vehicle or AM251, respectively (CA3: control,  $n = 18$ ; AM251,  $n = 22$ ; N.S.  $p = 0.97$ ; Tukey's post hoc). In contrast, the percent potentiation of LPP→DG synapses treated with AM251 stabilized at only 19.3 ± 6.2%, a value that was substantially reduced from that for LPP→CA3 (DG,  $n = 9$ ;  $F_{(3,51)} = 7.18$ ;  $p = 0.001$ ; Tukey's post hoc) or from vehicle-treated LPP→DG synapses ( $p = 0.003$ ; Fig. 4A–C). The latter result accords well with previous work on the effects of the CB1R inverse agonist on LTP in the LPP→DG connection (Wang et al., 2016). In all, the retrograde (spine to terminal) endocannabinoid signal used to generate presynaptic LTP in the DG does not play a role in LPP→CA3 potentiation, which is in agreement with the argument that LTP in the latter is expressed postsynaptically.

The rapid onset of the fEPSPs measured in the above experiments strongly suggests that polysynaptic (DG→CA3→CA3) activation of the massive CA3 collateral projections to *str.*

*radiatum* (Witter, 2007) did not contribute to the responses. It is possible however that the CA3 recurrent collateral system contributed to the net depolarization of the target dendrites during the theta bursts used to induce potentiation and thereby promoted LTP. To test this, we ran a group of slices ( $n = 10$ ) in which the MFs (DG→CA3) were severed at the level of their exit from the hilus of the DG (Figs. 1A, 4D). The percent LPP→CA3 potentiation in these cases was not reliably different from that recorded from intact slices (intact, 44.8 ± 4.6%; MF cut, 37.9 ± 5.5%;  $t_{(16)} = 0.909$ ;  $p = 0.377$ ; unpaired Student's  $t$  test) and AM251 again did not measurably affect LTP (34.8 ± 4.9%;  $t_{(9)} = 0.415$ ,  $p = 0.688$ ; vs controls, unpaired Student's  $t$  test; Fig. 4E).

CB1Rs on LPP→DG terminals exhibit an atypical form of signaling when activated by the agonist WIN (Chiu and Castillo, 2008; Wang et al., 2018b). Rather than depressing glutamate release, as is the case at most sites, the treatment has no influence

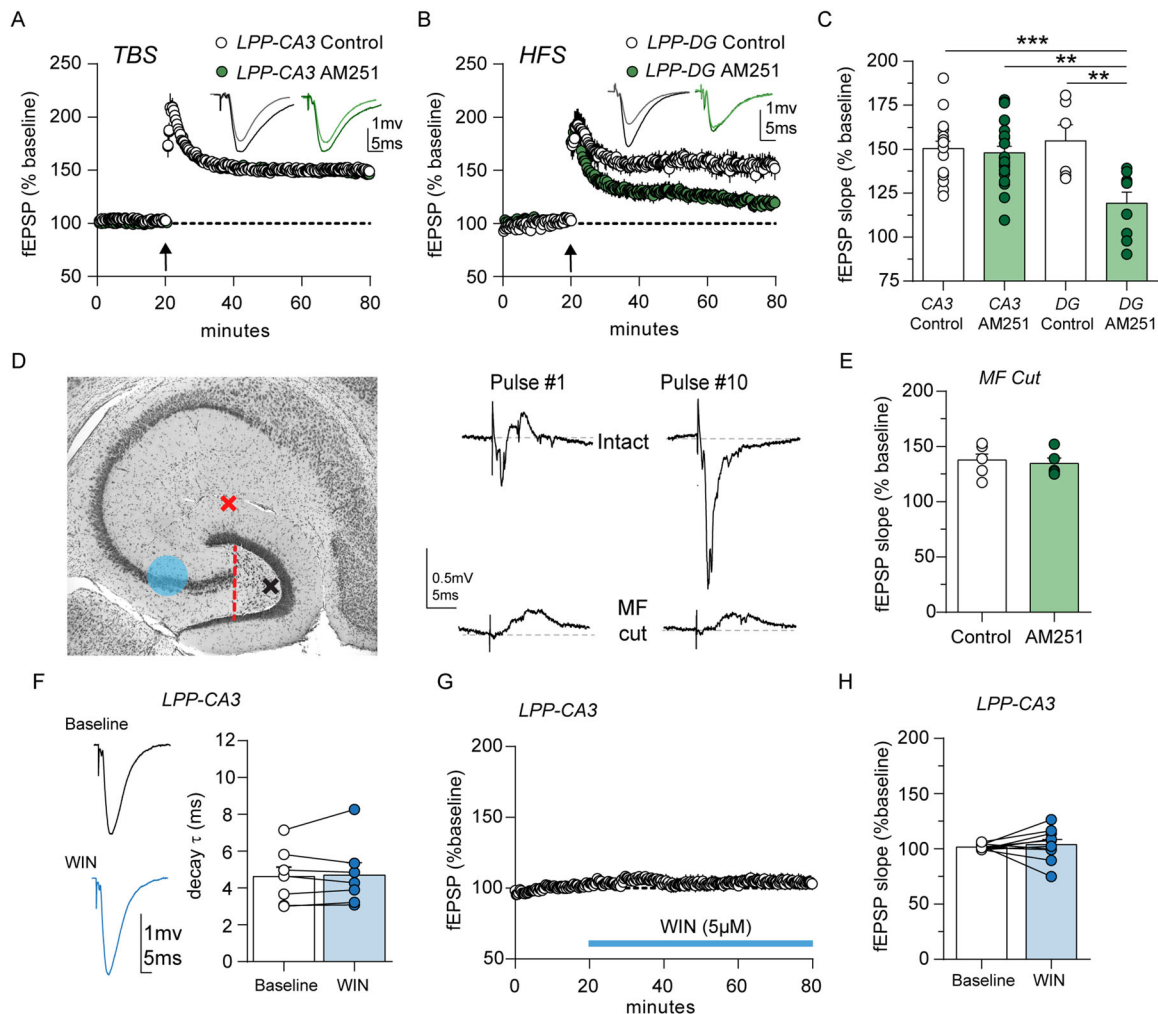


**Figure 4.** LPP→CA3 LTP does not require endocannabinoid signaling. **A**, Infusion of CB1R inverse agonist AM251 (5 μM) had no effect on TBS-induced LTP of LPP→CA3 synapses. Representative traces show LPP-evoked responses in CA3 before (light line) and 60 min after LTP induction (dark line) in the absence (black) and presence (green) of AM251 (18 slices/group). **B**, Infusion of AM251 disrupts HFS-induced LTP of LPP→DG synapses. Representative traces show LPP-evoked responses in the DG before (light line) and 60 min after LTP induction (dark line) in the absence (black) and presence (green) of AM251 (8 slices/group). **C**, Plot shows that at 60 min the magnitude of LTP (fEPSP slope) was unaffected by AM251 for LPP→CA3 synapses but was significantly lower for LPP→DG synapses ( $F_{(3,51)} = 7.18$ ;  $**p = 0.001$ ; Tukey's post hoc; one-way ANOVA interaction;  $**p < 0.01$ ). **D**, Left, Nissl-stained cross section of the temporal hippocampus illustrates location of the surgical cut that severed the MFs (red dashed line) and the position of the recording (shaded) and stimulating (X; red, LPP→DG; black, DG→CA3) electrodes. Right, Representative traces recorded from MF→CA3 synapses in response to a 10-pulse 20 Hz stimulation in an intact slice (top) and those with the MF cut (bottom). **E**, MF transection had no effect on the magnitude of LPP→CA3 LTP or the lack of AM251 vulnerability (control,  $n = 6$ ; AM251  $n = 5$ ;  $t_{(9)} = 0.42$ ,  $p = 0.68$ , unpaired Student's  $t$  test). **F**, Left, Representative LPP-evoked responses in the absence (black) and presence (blue) of CB1 receptor agonist WIN55-212-1 (5 μM, WIN). Right, Graph illustrating the mean fEPSP decay tau before and after 60 min WIN infusion ( $n = 7$ /group;  $t_{(6)} = 0.44$ ;  $p = 0.67$ ). **G**, WIN infusion did not influence the slope of LPP-evoked fEPSPs (103.96 ± 3.13). **H**, Graph comparing the mean responses during the last 5 min of baseline and the last 5 min of WIN infusion (55–60 min) for individual slices ( $n = 10$ /group;  $t_{(9)} = 0.49$ ;  $p = 0.63$ ).



on baseline transmission (Wang et al., 2016, 2018b). Similar to results for the DG (Wang et al., 2016), a 1 h infusion of the CB1R agonist WIN had no evident effect on the decay  $\tau$  (Fig. 4F) or initial slope (Fig. 4G,H) of the fEPSP elicited in CA3 by stimulation of the LPP. The slope, normalized to the mean 20 min drug-free baseline response, was  $104.0 \pm 3.1\%$  at the end of WIN infusion (baseline vs WIN,  $t_{(9)} = 0.494$ ;  $n = 10$ ;  $p = 0.633$ ; paired  $t$  test; Fig. 4H). Thus, while LPP terminals in CA3 do not rely upon endocannabinoids for the stabilization of LTP, they nonetheless resemble LPP→DG terminals with regard to the lack of baseline responses to CB1R agonists.

### LPP LTP stabilization in CA3 requires postsynaptic adjustments

The absence of evidence for presynaptic LTP expression or retrograde endocannabinoid actions at LPP→CA3 synapses reinforces the conclusion that in this field, LPP LTP is induced and expressed in the postsynaptic compartment. Thus, mechanisms could be comparable to those at the CA3→CA1 connection in which LTP expression involves an expansion of the postsynaptic density and stabilization is achieved by reorganization of the subsynaptic actin cytoskeleton (Kim and Lisman, 1999; Krucker et al., 2000; Kramar et al., 2006). We tested this idea by infusing Lat-A (400 nM), a toxin that blocks actin filament assembly, into CA3 pyramidal neurons before attempting to induce LPP→CA3 LTP. Such delivery of the toxin via clamp electrodes blocks LTP consolidation in CA1 (Kramar et al., 2006; Rex et al., 2007) but has no effect on any aspect of LPP potentiation in DG granule cells (Wang et al., 2016). The latter result is consistent with a presynaptic locus for expression and stabilization of potentiation.

We used the whole-cell voltage-clamp configuration to record LPP-evoked EPSCs (eEPSCs) from CA3 pyramidal cells ( $V_{\text{clamp}}, -70$  mV) using a stimulating electrode localized in distal *str. moleculare*. The amplitude and decay time course of LPP eEPSCs were unaffected by Lat-A in the recording pipette (Fig. 5A–C), an effect consistent with previous studies of DG granule cells and CA1 pyramidal cells (Wang et al., 2016). Two trains of TBS produced an immediate potentiation in control experiments that decayed over 10 min to a plateau value at  $176 \pm 3.8\%$  above pre-TBS baseline. Paired-pulse responses collected using 40 ms intervals were more variable across slices than was the case for field potentials, but mean percent facilitation was not reliably different before ( $72.1 \pm 19.5\%$ ) versus after ( $70.1 \pm 22.4\%$ ;  $R = 0.823$ ) induction of LTP. The initial potentiation was normal in Lat-A cases but potentiation decayed toward baseline over 25–30 min (Fig. 5D). The difference in percent LTP recorded at 45 min post-TBS for the two groups was highly significant ( $156 \pm 1.8\%$  vs  $97 \pm 2.1\%$ ;  $p < 0.001$ ; unpaired  $t$  test). The effects of intracellular application of Lat-A to CA3 neurons were similar to those described for CA1 and are indicative of postsynaptic expression of LTP at this synapse.

### Frequency facilitation differs at the two termination sites of the LPP

The marked differences in LTP between the two sets of LPP synapses raise the question of whether differentiation is specific to the complex events required to modify synapses or instead is evident for simpler levels of function. We therefore tested if the CA3 branch of the LPP expresses the unusual frequency facilitation described for LPP→DG contacts.

Prior studies showed that theta frequency (5 Hz) stimulation of LPP→DG synapses produces a small ( $\sim 5$ – $10\%$ ) within-train

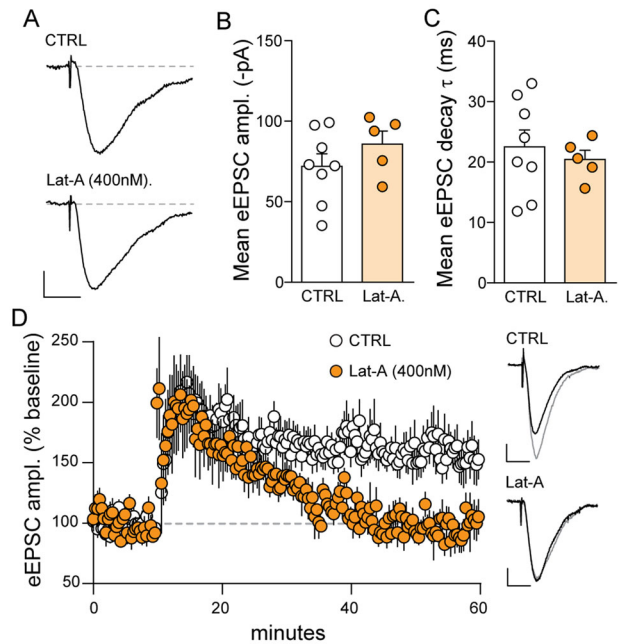


**Figure 5.** Postsynaptic Lat-A infusion prevents stabilization of LPP→CA3 LTP without effect upon baseline transmission. **A**, Ensemble averages of LPP→eEPSCs recorded from representative CA3 pyramidal cells in control (CTRL) cells and those receiving intracellular Lat-A infusion (scale bars:  $y = 20$  pA;  $x = 20$  ms). Lat-A had no effect upon the amplitude (**B**) or decay time  $\tau$  (**C**) of LPP eEPSCs. **D**, Postsynaptic Lat-A infusion blocked TBS-induced LTP at the LPP→CA3 synapse (CTRL,  $156 \pm 1.8\%$ ; Lat-A,  $97 \pm 2.1\%$ ;  $p < 0.001$ ). Right, Ensemble averages of LPP eEPSCs recorded from CA3 pyramidal cells before (black) and after LTP induction (gray) for control and Lat-A-treated cells (scale bars:  $y = 20$  pA;  $x = 20$  ms).

facilitation of fEPSPs (Trieu et al., 2015; Quintanilla et al., 2022), whereas a short train of 50 Hz stimulation generates an unusual pattern in which an initial facilitation is followed by a marked depression of the postsynaptic response (Amani et al., 2021; Le et al., 2022; Quintanilla et al., 2022). Our recent analyses indicate that this frequency following profile is primarily due to release dynamics with little if any contribution from postsynaptic variables (Quintanilla et al., 2022). For the CA3 branch of the LPP, theta frequency facilitation was clearly greater than in the DG segment: an initial  $\sim 20\%$  increase in fEPSP slope persisted throughout a 10-pulse train (pulse 10:  $115.2 \pm 5.4\%$ ;  $n = 14$ ). A somewhat larger initial facilitation was elicited by beta frequency (20 Hz) stimulation ( $176.61 \pm 6.08\%$  for pulse 2), but in this instance the enhancement steadily decreased from the third pulse onward (pulse 10,  $126.54 \pm 6.64\%$ ;  $n = 14$ ). A similar but considerably exaggerated pattern was produced by 50 Hz stimulation: the initial enhancement ( $161.81 \pm 6.38\%$  for pulse 2) was comparable with that produced by 20 Hz but the loss of facilitation was greater with the responses falling below baseline later in the train (pulse 10,  $90.89 \pm 3.48\%$ ;  $n = 13$ ; Fig. 6A,B). These frequency curves are qualitatively similar to those described for LPP→DG synapses (Quintanilla et al., 2022) but with a greater initial facilitation and a lesser within-train decline.

A possible complication for the above analyses involves contributions from the CA3 associational system to the size or waveform of LPP elicited fEPSPs in *str. moleculare*. This could occur if LPP→DG stimulation engaged enough MFs to trigger spiking in a large number of CA3 pyramidal cells. The CA3 axon collaterals terminate proximal to the dendritic targets of the LPP and might therefore generate potentials that contaminate those from the latter projection. However, severing the MFs as they exit the hilus

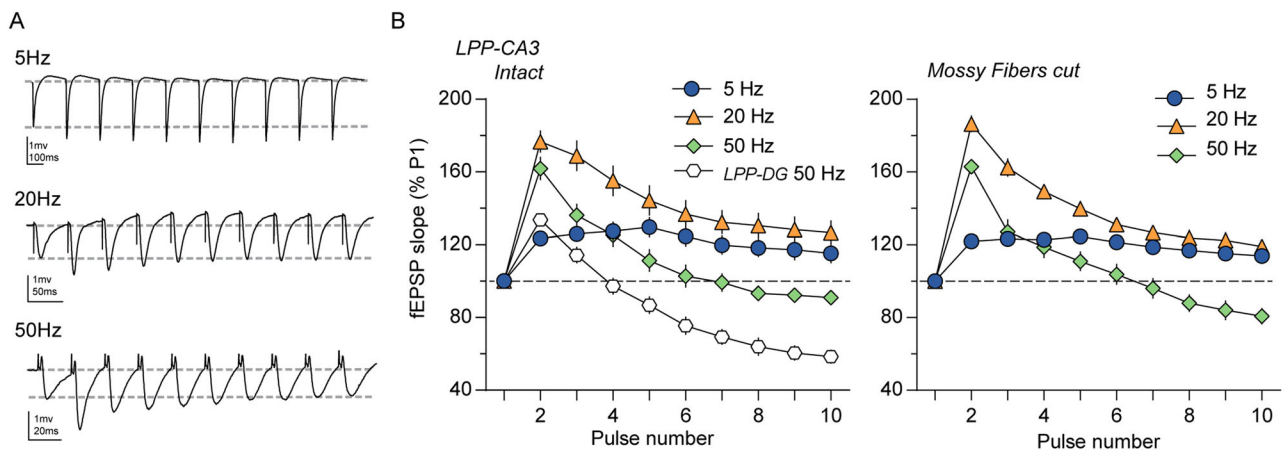


**Figure 6.** LPP→CA3 responses are frequency dependent. **A**, Representative traces recorded from CA3 str. lacunosum in response to LPP stimulation (10 pulses) at 5, 20, and 50 Hz. **B**, Graph summarizing the within-train facilitation of the LPP→CA3 fEPSP slope for each stimulation frequency recorded from intact slices (left) and slices in which the MF connection with CA3 had been severed (right).

(Figs. 1A, 4D) had no reliable effect on frequency facilitation elicited by 5, 20, or 50 Hz stimulation of the LPP (5 Hz pulse 10,  $113.93 \pm 2.12\%$ ; 20 Hz pulse 10,  $119.08 \pm 4.07\%$ ; 50 Hz pulse 10,  $80.82 \pm 4.51\%$ ;  $n = 14$ ; Fig. 6B).

### Presynaptic factors may contribute to differences in frequency facilitation at the two populations of LPP terminals

The PPR results together with the upward displacement of the frequency facilitation curves for LPP→CA3 relative to LPP→DG synapses constitute evidence for target specification of release properties of LPP terminals. We used Monte Carlo simulations of a two-step release model (Miki et al., 2016) to search for presynaptic variables that might underlie the differences in the frequency facilitation profiles of the two LPP branches. The model incorporates factors associated with the release and the subsequent replenishment of synaptic vesicles including probability of vesicle docking ( $\delta$ ), release probability of a docked vesicle ( $p_v$ ), probability of a vesicle transitioning to a vacant docking site from the replacement pool ( $r$ ), and replacement pool replenishment ( $s$ ). The overall release probability ( $p$ ) is the product of  $\delta$  and  $p_v$  (Fig. 7A and Materials and Methods). Given that the primary difference observed electrophysiologically between the two LPP synapses related to  $p$  (i.e., differences in PPR), we first used our previously optimized parameters for the simulated LPP→DG synapse (Quintanilla et al., 2022; Fig. 7A) and tested if simply lowering  $p$  (i.e., all other parameters unchanged) was sufficient to recapitulate the LPP→CA3 responses to 50 Hz input (see Materials and Methods). Decreasing the net release probability  $p$  (i.e.,  $\delta p_v$ ) from 0.33 to 0.25, 0.20, or 0.16 caused a progressive increase in the initial facilitation and a reduction in the subsequent suppression of responses during the train (Fig. 7B). Reducing  $p$  to a value of 0.25 changed the simulated LPP→DG pattern into one that approximated the recorded 50 Hz curve for LPP→CA3 synapses. The selective optimization of  $\delta$  and  $p_v$  such that they no longer provided an equal contribution to  $p$  generated output curves that aligned more closely with the electrophysiological data recorded from intact slices as well as those lacking the MF connection (i.e., MF cut; Fig. 7C,D; intact:  $p = 0.25$ , SE = 0.030; MF cut:  $p = 0.22$ , SE = 0.035). The similarity between the simulated MF cut and intact frequency curves adds support to the conclusion that recruitment of the MF input to CA3 is unlikely to

contribute significantly to the output profile recorded from the LPP→CA3 synapse.

Given these observations, we next tested further how the composition of the overall  $p$  (i.e., relative contribution of  $\delta$  and  $p_v$ ) influences the simulated output profile. To do this, we configured the model to have a  $p$  of 0.22, which was generated with either  $\delta = 0.4$  and  $p_v = 0.55$  or  $\delta = 0.55$  and  $p_v = 0.4$  (see Materials and Methods). Under these two configurations, the simulated output curves were noticeably different (Fig. 7E). This suggests that subtle manipulations of processes associated with vesicle docking or the release probability of docked vesicles may differentially influence the operations at a given synapse. Specifically, decreasing  $\delta$  produces a significantly larger initial facilitation, in accord with an observed difference between the terminals of two branches of the LPP. We then tested how reliably the model recapitulated the experimental data when the overall  $p$  was reduced by selectively decreasing  $\delta$  only. Under such conditions, the initial phase of the simulated output profile aligned closely with the electrophysiological data, but the within-train suppression evident later in the train was exaggerated (Fig. 7F). A parameter optimization revealed that selectively decreasing  $\delta$  could reliably reproduce the empirical output curves when the probability of replacement pool replenishment (i.e.,  $s$ ) was additionally increased from 0.4 to 0.5 (Fig. 7F).

The model thus suggests that the different output profiles expressed by the two branches of the LPP may result from surprisingly modest differences (i.e., only two variables) in release dynamics and vesicle recycling.

### The two-step model predicts the effects of increasing $p$ upon the output profile following 50 Hz stimulation

The above simulations identified parameters that reproduce with reasonable accuracy the observed responses elicited at the two LPP terminals by a train of pulses at 50 Hz. We then asked if the resultant model could predict the results obtained with an experimental manipulation known to modify certain parameters. Phorbol esters exert potent effects on transmitter release at many sites (Silinsky and Searl, 2003) including a number of synapses within the hippocampus (Muller and Lynch, 1988; Honda et al., 2000; Aldahabi et al., 2022). Such an effect on release dynamics has primarily been ascribed to activation of munc-13, a presynaptic protein critical for vesicle priming, and

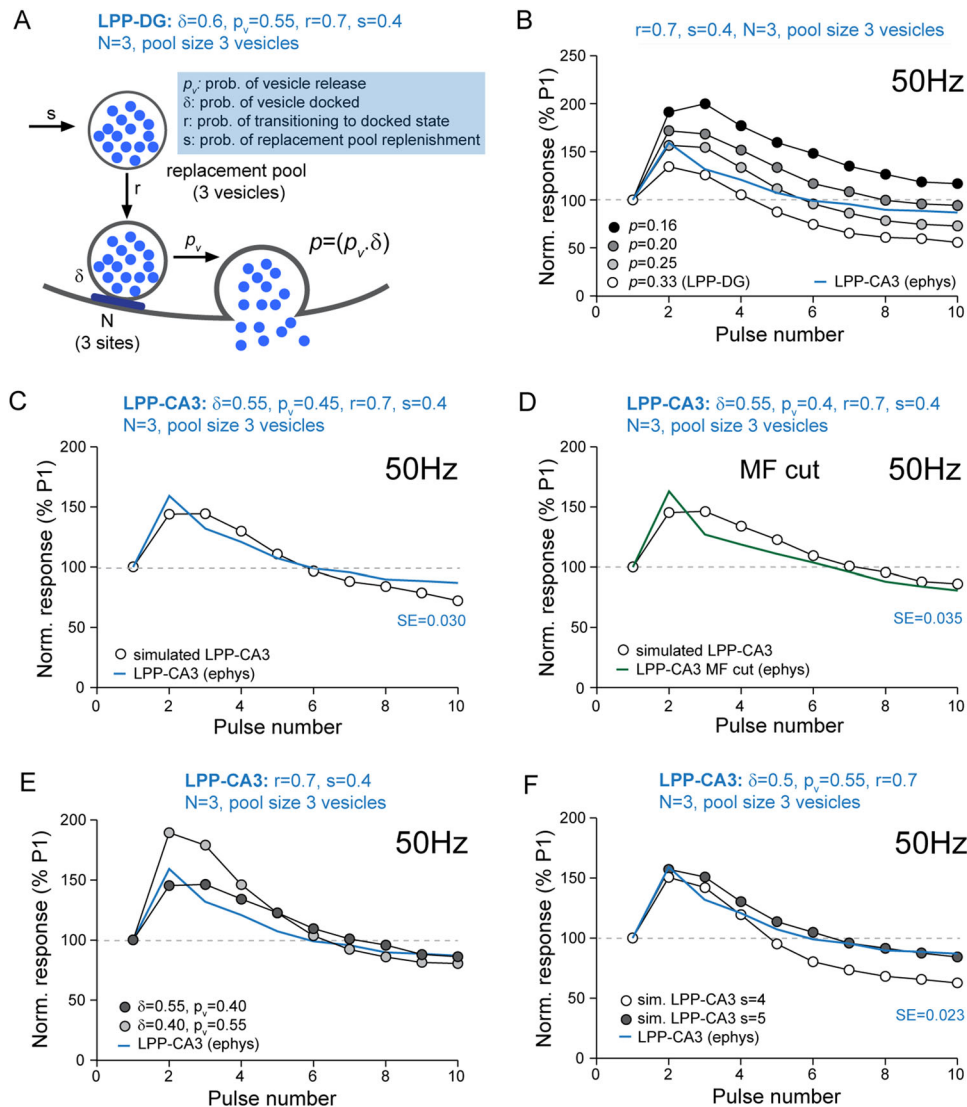


**Figure 7.** Differences in release dynamics may underlie differences in frequency facilitation between the two branches of the LPP. **A**, Schematic illustration of the two-step release model, where  $N$  describes the number of docking sites. **B**, Selectively decreasing  $p$  in the physiologically constrained two-step release model increased the initial facilitation and reduced within-train suppression observed in the simulated LPP→DG output curve with 50 Hz LPP stimulation. Note that decreasing  $p$  to 0.25 crudely recapitulated the empirical LPP→CA3 output profile (blue line). Optimization of the release dynamics,  $\delta$  and  $p_v$ , produced an output curve more analogous to the electrophysiological data recorded from the intact slice (**C**) and in slices with the MF cut (**D**). The empirical data for intact (**C**, blue line) and MF cut (**D**, green line) slices are illustrated. **E**, The relative contribution of  $\delta$  and  $p_v$  to the overall  $p$  is critical for determining the magnitude of the initial facilitation and within-train suppression of the simulated output profile following 50 Hz stimulation. **F**, Using a model where  $\delta$  is selectively reduced, the electrophysiological LPP→CA3 output profile (blue line) can be largely recapitulated by increasing  $s$ .

subsequent increase in  $p$  (Betz et al., 1998; Rizo, 2018). Accordingly, the effects of a phorbol ester upon  $p$  were approximated by increasing the probability of a vesicle occupying a release site ( $\delta$ ) and releasing its contents ( $p_v$ ; see Materials and Methods). The remaining parameters within the model were left unchanged. The “phorbol” adjustments increased the initial responses of the LPP→DG synapses but had surprisingly little effect on the progressive decrease in evoked fEPSPs during the remainder of the train. The net result was a loss of the facilitation followed by a strong depression pattern that normally occurs during a gamma train (Fig. 8A). This indicates that the dynamics for replacement and replenishment of vesicles play a much larger role than docking and exocytosis in shaping the behavior of the model as a high-frequency input train continues. The simulated CA3 responses with phorbol-related parametric changes resembled those for the DG except that the facilitation of response 2

over response 1, seen under baseline conditions, was still present. Importantly, the reduction in responses as the train proceeded did not turn into outright depression, as was the case for the DG (Fig. 8B). Predictions from these simulations were largely confirmed in experimental work. A low concentration (1  $\mu$ M) of the phorbol ester, PDBU, increased the LPP→DG fEPSP to a greater degree than predicted but the loss of within-train facilitation and rapid conversion into depression were qualitatively and quantitatively comparable with those in the simulation (Fig. 8C). There was close agreement between simulation and experiment for the LPP→CA3 connection. The percent PDBU-induced enhancement of the initial response was almost identical to that in the model as was the retained facilitation of response 2 over response 1. The decline of within-train responses was slightly less pronounced in experiments but endpoint (pulse 10) values were very close (Fig. 8D).

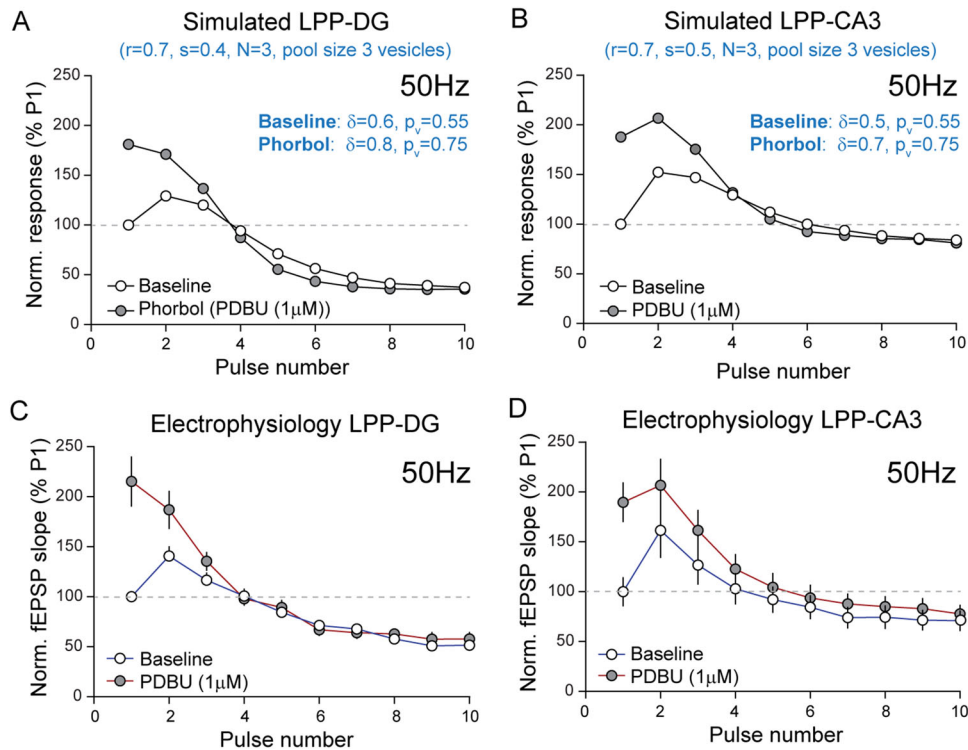


**Figure 8.** The simulated two-step release model predicts the effects of the phorbol ester, PDBU upon the output profile with 50 Hz stimulation at LPP→DG and LPP→CA3 synapses. Graphs summarizing the predicted effects that the phorbol ester (PDBU)-induced increase in  $p$  has upon the output curve following 50 Hz stimulation at LPP→DG (**A**) and LPP→CA3 (**B**) terminals. The empirically measured effects of PDBU (1  $\mu$ M) treatment upon the output profile recorded from LPP→DG (**C**) and LPP→CA3 (**D**) terminals during a 10-pulse, 50 Hz LPP stimulation are similar to those predicted by the simulation.

## Discussion

The present studies addressed a basic and largely unexplored question regarding memory-related synaptic plasticity: does the pre- or postsynaptic side of a synaptic contact determine the locus of LTP expression and stabilization. Prior studies showed that the pyramidal cell→pyramidal cell synapses formed by the CA3→CA1 projection use a postsynaptic form of LTP (Kauer et al., 1988; Muller and Lynch, 1988; Manabe and Nicoll, 1994; Rex et al., 2009; Granger and Nicoll, 2014). However, the somewhat different pyramidal cells in lateral EC (Witter et al., 2017) generate a presynaptic variant at their LPP connections with the DG granule cells (Wang et al., 2016). If the postsynaptic cell dictates the form of potentiation, then we would expect the CA3 (pyramidal cell) branch of the LPP to express a postsynaptic LTP variant. On the other hand, if the afferent axons impose the form of potentiation independent of the target cell type, one would expect the LPP→CA3 synapses to express presynaptic LTP similar to that described for LPP→DG contacts. The results indicate that LTP at LPP→CA3 contacts is similar to that in CA1, resulting in pre- and postsynaptic forms of LTP being expressed by the same LPP axons.

The above conclusion is supported by results obtained using the two stimulation protocols—theta bursts and high-frequency trains—conventionally employed to induce LTP. The question thus arises of whether other induction conditions might shift the locus of potentiation at either or both branches of the LPP. A recent study showed that a particular spiking response by granule cells is required for the production of LTP in the LPP→DG connection (Kim et al., 2023). This suggests that input pattern is important only so far as it elicits an appropriate induction signal in the target cell. The same experiments showed that LTP was

much more readily induced in a biophysically defined subpopulation of granule neurons. It will be useful in future work to expand the analysis of response requirements and cell types to include a broader range of stimulation patterns and tests for pre- versus postsynaptic sites of expression. This could allow for detection of currently unknown rules governing the categories of LTP expressed by the two targets of the LPP.

Conversely, multiple lines of evidence point to the conclusion that the two sets of LPP connections have different competencies with regard to activity-driven modifications. For both sites, LTP is blocked by NMDAR antagonists and by buffering intracellular calcium postsynaptically (Lynch et al., 1983; McMahon and Barrionuevo, 2002; Wang et al., 2016), indicating that the initial triggering steps for the two forms of potentiation are located in the postsynaptic element. There is however evidence for substantial differences in the locus of LTP expression and stabilization in LPP→DG versus LPP→CA3 contacts. Experiments using genomic manipulations, toxins, peptide antagonists, and imaging have shown that a subgroup of integrin adhesion receptors are located in the postsynaptic density of CA1 spine synapses and required for LTP stabilization (Chan et al., 2006; Kramar et al., 2006; Babayan et al., 2012). CA1 and CA3 have the same general pattern of integrin expression, whereas the DG granule cells produce a very unusual (for brain)  $\alpha$ 4 $\beta$ 7 subunit combination (Pinkstaff et al., 1999). Integrins regulate the cytoskeleton (Wiesner et al., 2005) and CA1 LTP requires  $\beta$ 1 integrin-dependent actin polymerization in spines. Intracellular application of Lat-A, a toxin, that blocks theta burst induced assembly of actin filaments, disrupts LTP in CA1 (Kramar et al., 2006; Rex et al., 2007) and, as shown here, in CA3. The same treatment applied to granule cells had no effect on LPP→DG potentiation

(Wang et al., 2016). These observations raise the possibility that an  $\alpha 4\beta 7$  integrin found in granule neurons is either not engaged by high-frequency afferent activity or is incapable of mediating the spine cytoskeletal reorganization required for postsynaptic LTP. In this scenario, the LPP projections to CA3 have access to the same integrins present in CA1 and thus to the actin signaling required for postsynaptic LTP. An implication of this argument is that LTP in the MPP and commissural/associational projections to the DG will express presynaptic versions of LTP. The pre- versus postsynaptic locus of potentiation has not been resolved for the MPP, but detailed studies by Castillo and colleagues indicate that LTP expression is presynaptic for the DG commissural/associational system (Hashimoto et al., 2017; Jensen et al., 2021).

Conversely, the LPP→CA3 contacts appear to lack most if not all of the features that generate or signify presynaptic LTP, at least as expressed at LPP→DG contacts. As noted, available evidence indicates that the enhanced release that underlies LPP→DG potentiation is triggered by on-demand endocannabinoid synthesis in granule cells followed by atypical signaling by CB1Rs located on LPP terminals (Wang et al., 2016, 2018b). The receptors generate a more conventional depression of release in CA1. In contrast to its effects on LPP→DG contacts, CB1R antagonism did not affect LTP in the CA3 branch of the LPP. But similar to their actions in the DG, CB1R agonists failed to produce the expected depression of release in LPP→CA3 contacts, suggesting that the endocannabinoid receptors on LPP terminals exhibit atypical signaling in both terminal fields. Why then did not patterned afferent stimulation generate the robust, endocannabinoid-dependent enhancement of release found in the DG? One possibility is that the brief periods of activation used to induce LTP fail to generate as robust a surge of postsynaptic endocannabinoid synthesis in CA3 as occurs in the DG. In this hypothesis, the CA3 endings possess the machinery for presynaptic LTP, but the ligand arriving from target spines is insufficient. Alternatively, target specification by pyramidal cell spines could reduce or eliminate one or more of the presynaptic signaling steps used by the presynaptic CB1Rs to produce a lasting increase in evoked release. The clear difference in frequency facilitation curves between the two LPP branches points to local regulation of terminal properties, and it is not unreasonable to suggest that this extends to the status of CB1R-initiated signaling cascades. It may be possible to distinguish between the “weak signal” versus “disrupted effector” models by testing if CB1R agonists activate LTP-critical signaling steps (e.g., RhoA kinase phosphorylation; Wang et al., 2018b) in LPP→CA3 terminals to the extent observed for LPP→DG terminals. Evidence that the essential ingredients for presynaptic LTP are present in CA3 would again raise the question of whether there are afferent patterns that could trigger this form of potentiation.

The use of distinctly different forms of plasticity by the same afferent will likely have important effects on the encoding of information by hippocampus. The much discussed “synaptic tagging” effect constitutes an important example of this (Frey and Morris, 1997; Redondo and Morris, 2011). As recorded in CA1, tagging involves facilitation of LTP via the delivery of plasticity-related proteins, from activated synapses to contacts that had been stimulated at an earlier time point. The effect requires intradendritic transfer of material from one set of synapses to another and accordingly would be operational only in cells that utilize postsynaptic LTP. It follows from this that tagging most likely can occur in the LPP→CA3 connection but not in the LPP→DG projection. Relatedly, recent studies have linked interactions between spines to a LTP “spaced trials

effect” in which a second TBS train doubles the magnitude of CA1 LTP produced by a first train when the two stimulation episodes are separated by at least 1 h (Kramar et al., 2012; Cao and Harris, 2014). Studies indicate that synapses in hippocampus can have low or high plasticity thresholds and that induction of LTP in the former primes the latter for induction of the potentiated state, with protein transfer between spines being the requisite exchange process (Lynch et al., 2013). The production of a spaced trials effect for LTP—which has been linked to learning (Seese et al., 2014)—in the LPP would accordingly be expected to be much greater in CA3 than that in the DG.

The functional consequences of two forms of LTP will likely be affected by the sizeable differences in frequency facilitation between the two LPP branches. The latter findings constitute the first evidence that information carried by single cortical axons will be preferentially routed to CA3 via the direct as opposed to the indirect (LPP→DG→CA3) path due to the blunting of DG responses to gamma frequency (>50 Hz) activation. An appreciation of those aspects of release dynamics that account for differences between the two sites could be an important step toward determining the spine-to-terminal specification mechanism. Simulation results identified likely candidates for the kinetic features that differed between the two LPP termination sites, but a more precise description is possible. Specifically, recent studies have reported that expanding the two-step vesicle release model (Miki et al., 2016) to incorporate two reversible vesicle priming states, termed tightly (i.e., primed) and loosely docked (TS and LS, respectively), enabled the simulated output to reliably recapitulate experimentally derived output curves recorded from the calyx of Held (Lin et al., 2022). The relative proportion of docked synaptic vesicles occupying the primed, TS state has been postulated as a critical determinant in the frequency-dependent operations of a given synapse (Neher and Brose, 2018; Lin et al., 2022). As such, synapses containing a high proportion of TS vesicles typically have a high initial  $p$ , displaying short-term depression of responses following high-frequency activation, while those synapses comprised primarily of LS vesicles exhibit a low  $p$  and frequency facilitation (Neher and Brose, 2018; Aldahabi et al., 2022; Lin et al., 2022). Indeed, it has recently been proposed that different vesicle priming states underpin postsynaptic target cell differences in synaptic efficacy associated with CA1 pyramidal cell innervation of specific interneuron subtypes (Aldahabi et al., 2022). Consistent with this notion, selectively reducing the probability of vesicles being docked ( $\delta$ ), which, in our two-step model is a factor associated with vesicle priming, and modestly increasing the recycling of vesicles to the replacement pool ( $s$ ) transformed the simulated output from the LPP→DG synapse to one more comparable to LPP→CA3 contacts. This suggests that relatively subtle differences in vesicle priming and recycling may explain the functional differences in synaptic transmission in the two LPP terminal fields. Synaptotagmin 3 is a  $\text{Ca}^{2+}$  sensing protein postulated to promote frequency facilitation by driving the transition of synaptic vesicles to their primed state as well as by increasing replenishment of the readily releasable pool (Weingarten et al., 2022). As such it is an attractive candidate for the presynaptic element differentially regulated by granule versus pyramidal cells. The differences in frequency facilitation curves, although described by a single set of parameters here, may in reality reflect a combination of terminals with mixed release properties (i.e.,  $p$  and vesicle recycling). Previous studies demonstrated that a mixture of high and low  $p$  terminals could recapitulate the LPP→DG output profile to 50 Hz stimulation (Quintanilla et al., 2022), and it is not

unreasonable to assume that subtle alterations in the contribution of such terminals may contribute to the different output profile observed at LPP→CA3 terminals.

## References

- Aldahabi M, Balint F, Holderith N, Lorincz A, Reva M, Nusser Z (2022) Different priming states of synaptic vesicles underlie distinct release probabilities at hippocampal excitatory synapses. *Neuron* 110:4144–4161.e7.
- Amani M, Lauterborn JC, Le AA, Cox BM, Wang W, Quintanilla J, Cox CD, Gall CM, Lynch G (2021) Rapid aging in the perforant path projections to the rodent dentate gyrus. *J Neurosci* 41:2301–2312.
- Amaral DG (1993) Emerging principles of intrinsic hippocampal organization. *Curr Opin Neurobiol* 3:225–229.
- Amaral DG, Ishizuka N, Claiborne B (1990) Neurons, numbers and the hippocampal network. *Prog Brain Res* 83:1–11.
- Babayan AH, et al. (2012) Integrin dynamics produce a delayed stage of long-term potentiation and memory consolidation. *J Neurosci* 32:12854–12861.
- Bao J, Reim K, Sakaba T (2010) Target-dependent feedforward inhibition mediated by short-term synaptic plasticity in the cerebellum. *J Neurosci* 30:8171–8179.
- Berzhanskaya J, Urban NN, Barrionuevo G (1998) Electrophysiological and pharmacological characterization of the direct perforant path input to hippocampal area CA3. *J Neurophysiol* 79:2111–2118.
- Betz A, Ashery U, Rickmann M, Augustin I, Neher E, Sudhof TC, Rettig J, Brose N (1998) Munc13-1 is a presynaptic phorbol ester receptor that enhances neurotransmitter release. *Neuron* 21:123–136.
- Cao G, Harris KM (2014) Augmenting saturated LTP by broadly spaced episodes of theta-burst stimulation in hippocampal area CA1 of adult rats and mice. *J Neurophysiol* 112:1916–1924.
- Castillo PE, Younts TJ, Chavez AE, Hashimoto-dani Y (2012) Endocannabinoid signaling and synaptic function. *Neuron* 76:70–81.
- Chan CS, Weeber EJ, Zong L, Fuchs E, Sweatt JD, Davis RL (2006) Beta 1-integrins are required for hippocampal AMPA receptor-dependent synaptic transmission, synaptic plasticity, and working memory. *J Neurosci* 26:223–232.
- Chen LY, Rex CS, Casale MS, Gall CM, Lynch G (2007) Changes in synaptic morphology accompany actin signaling during LTP. *J Neurosci* 27:5363–5372.
- Chiu CQ, Castillo PE (2008) Input-specific plasticity at excitatory synapses mediated by endocannabinoids in the dentate gyrus. *Neuropharmacology* 54:68–78.
- Christie BR, Abraham WC (1994) Differential regulation of paired-pulse plasticity following LTP in the dentate gyrus. *Neuroreport* 5:385–388.
- Cox BM, Cox CD, Gunn BG, Le AA, Inshishian VC, Gall CM, Lynch G (2019) Acquisition of temporal order requires an intact CA3 commissural/associational (C/A) feedback system in mice. *Commun Biol* 2:251.
- Del Castillo J, Katz B (1954) Statistical factors involved in neuromuscular facilitation and depression. *J Physiol* 124:574–585.
- Eichenbaum H, Fortin NJ (2005) Bridging the gap between brain and behavior: cognitive and neural mechanisms of episodic memory. *J Exp Anal Behav* 84:619–629.
- Eichenbaum H, Sauvage M, Fortin N, Komorowski R, Lipton P (2012) Towards a functional organization of episodic memory in the medial temporal lobe. *Neurosci Biobehav Rev* 36:1597–1608.
- Frey U, Morris RG (1997) Synaptic tagging and long-term potentiation. *Nature* 385:533–536.
- Granger AJ, Nicoll RA (2014) Expression mechanisms underlying long-term potentiation: a postsynaptic view, 10 years on. *Philos Trans R Soc Lond B Biol Sci* 369:20130136.
- Gunn BG, Cox CD, Chen Y, Frotscher M, Gall CM, Baram TZ, Lynch G (2017) The endogenous stress hormone CRH modulates excitatory transmission and network physiology in hippocampus. *Cereb Cortex* 27:4182–4198.
- Hargreaves EL, Rao G, Lee I, Knierim JJ (2005) Major dissociation between medial and lateral entorhinal input to dorsal hippocampus. *Science* 308:1792–1794.
- Hashimoto-dani Y, Nasrallah K, Jensen KR, Chavez AE, Carrera D, Castillo PE (2017) LTP at hilar mossy cell-dentate granule cell synapses modulates dentate gyrus output by increasing excitation/inhibition balance. *Neuron* 95:928–943.e3.
- Henze DA, Wittner L, Buzsaki G (2002) Single granule cells reliably discharge targets in the hippocampal CA3 network in vivo. *Nat Neurosci* 5:790–795.
- Honda I, Kamiya H, Yawo H (2000) Re-evaluation of phorbol ester-induced potentiation of transmitter release from mossy fibre terminals of the mouse hippocampus. *J Physiol* 529:763–776.
- Hunsaker MR, Chen V, Tran GT, Kesner RP (2013) The medial and lateral entorhinal cortex both contribute to contextual and item recognition memory: a test of the binding of items and context model. *Hippocampus* 23:380–391.
- Jackman SL, Regehr WG (2017) The mechanisms and functions of synaptic facilitation. *Neuron* 94:447–464.
- Jensen KR, Berthouex C, Nasrallah K, Castillo PE (2021) Multiple cannabinoid signaling cascades powerfully suppress recurrent excitation in the hippocampus. *Proc Natl Acad Sci U S A* 118:e2017590118.
- Kano M, Ohno-Shosaku T, Hashimoto-dani Y, Uchigashima M, Watanabe M (2009) Endocannabinoid-mediated control of synaptic transmission. *Physiol Rev* 89:309–380.
- Katona I, Urban GM, Wallace M, Ledent C, Jung KM, Piomelli D, Mackie K, Freund TF (2006) Molecular composition of the endocannabinoid system at glutamatergic synapses. *J Neurosci* 26:5628–5637.
- Kauer JA, Malenka RC, Nicoll RA (1988) A persistent postsynaptic modification mediates long-term potentiation in the hippocampus. *Neuron* 1:911–917.
- Kim Y, Kim S, Ho WK, Lee SH (2023) Burst firing is required for induction of Hebbian LTP at lateral perforant path to hippocampal granule cell synapses. *Mol Brain* 16:45.
- Kim CH, Lisman JE (1999) A role of actin filament in synaptic transmission and long-term potentiation. *J Neurosci* 19:4314–4324.
- Kramar EA, Babayan AH, Gavin CF, Cox CD, Jafari M, Gall CM, Rumbaugh G, Lynch G (2012) Synaptic evidence for the efficacy of spaced learning. *Proc Natl Acad Sci U S A* 109:5121–5126.
- Kramar EA, Lin B, Rex CS, Gall CM, Lynch G (2006) Integrin-driven actin polymerization consolidates long-term potentiation. *Proc Natl Acad Sci U S A* 103:5579–5584.
- Krucker T, Siggins GR, Halpain S (2000) Dynamic actin filaments are required for stable long-term potentiation (LTP) in area CA1 of the hippocampus. *Proc Natl Acad Sci U S A* 97:6856–6861.
- Lauterborn JC, Kramar EA, Rice JD, Babayan AH, Cox CD, Karsten CA, Gall CM, Lynch G (2017) Cofilin activation is temporally associated with the cessation of growth in the developing hippocampus. *Cereb Cortex* 27:2640–2651.
- Lawrence JJ, Grinspan ZM, McBain CJ (2004) Quantal transmission at mossy fibre targets in the CA3 region of the rat hippocampus. *J Physiol* 554:175–193.
- Lawrence JJ, McBain CJ (2003) Interneuron diversity series: containing the detonation—feedforward inhibition in the CA3 hippocampus. *Trends Neurosci* 26:631–640.
- Le AA, Quintanilla J, Amani M, Piomelli D, Lynch G, Gall CM (2022) Persistent sexually dimorphic effects of adolescent THC exposure on hippocampal synaptic plasticity and episodic memory in rodents. *Neurobiol Dis* 162:105565.
- Lin KH, Taschenberger H, Neher E (2022) A sequential two-step priming scheme reproduces diversity in synaptic strength and short-term plasticity. *Proc Natl Acad Sci U S A* 119:e2207987119.
- Lynch G, Kramar EA, Babayan AH, Rumbaugh G, Gall CM (2013) Differences between synaptic plasticity thresholds result in new timing rules for maximizing long-term potentiation. *Neuropharmacology* 64:27–36.
- Lynch G, Larson J, Kelso S, Barrionuevo G, Schottler F (1983) Intracellular injections of EGTA block induction of hippocampal long-term potentiation. *Nature* 305:719–721.
- Manabe T, Nicoll RA (1994) Long-term potentiation: evidence against an increase in transmitter release probability in the CA1 region of the hippocampus. *Science* 265:1888–1892.
- Matsuda S, Kobayashi Y, Ishizuka N (2004) A quantitative analysis of the laminar distribution of synaptic boutons in field CA3 of the rat hippocampus. *Neurosci Res* 49:241–252.
- McMahon DB, Barrionuevo G (2002) Short- and long-term plasticity of the perforant path synapse in hippocampal area CA3. *J Neurophysiol* 88:528–533.
- McNaughton BL (1980) Evidence for two physiologically distinct perforant pathways to the fascia dentata. *Brain Res* 199:1–19.
- Miki T, Malagon G, Pulido C, Llano I, Neher E, Marty A (2016) Actin- and myosin-dependent vesicle loading of presynaptic docking sites prior to exocytosis. *Neuron* 91:808–823.

- Muller D, Lynch G (1988) Long-term potentiation differentially affects two components of synaptic responses in hippocampus. *Proc Natl Acad Sci U S A* 85:9346–9350.
- Muller D, Lynch G (1989) Evidence that changes in presynaptic calcium currents are not responsible for long-term potentiation in hippocampus. *Brain Res* 479:290–299.
- Neher E, Brose N (2018) Dynamically primed synaptic vesicle states: key to understand synaptic short-term plasticity. *Neuron* 100:1283–1291.
- Nicoll RA (2003) Expression mechanisms underlying long-term potentiation: a postsynaptic view. *Philos Trans R Soc Lond B Biol Sci* 358:721–726.
- Nicoll RA, Schmitz D (2005) Synaptic plasticity at hippocampal mossy fibre synapses. *Nat Rev Neurosci* 6:863–876.
- Petersen RP, Moradpour F, Eadie BD, Shin JD, Kannangara TS, Delaney KR, Christie BR (2013) Electrophysiological identification of medial and lateral perforant path inputs to the dentate gyrus. *Neuroscience* 252:154–168.
- Piette C, Cui Y, Gervasi N, Venance L (2020) Lights on endocannabinoid-mediated synaptic potentiation. *Front Mol Neurosci* 13:132.
- Pinkstaff JK, Detterich J, Lynch G, Gall C (1999) Integrin subunit gene expression is regionally differentiated in adult brain. *J Neurosci* 19:1541–1556.
- Quintanilla J, Jia Y, Lauterborn JC, Pruess BS, Le AA, Cox CD, Gall CM, Lynch G, Gunn BG (2022) Novel types of frequency filtering in the lateral perforant path projections to dentate gyrus. *J Physiol* 600:3865–3896.
- Reagh ZM, Yassa MA (2014) Object and spatial mnemonic interference differentially engage lateral and medial entorhinal cortex in humans. *Proc Natl Acad Sci U S A* 111:E4264–E4273.
- Rebola N, Carta M, Mulle C (2017) Operation and plasticity of hippocampal CA3 circuits: implications for memory encoding. *Nat Rev Neurosci* 18:208–220.
- Redondo RL, Morris RG (2011) Making memories last: the synaptic tagging and capture hypothesis. *Nat Rev Neurosci* 12:17–30.
- Rex CS, Chen LY, Sharma A, Liu J, Babayan AH, Gall CM, Lynch G (2009) Different Rho GTPase-dependent signaling pathways initiate sequential steps in the consolidation of long-term potentiation. *J Cell Biol* 186:85–97.
- Rex CS, Lin CY, Kramar EA, Chen LY, Gall CM, Lynch G (2007) Brain-derived neurotrophic factor promotes long-term potentiation-related cytoskeletal changes in adult hippocampus. *J Neurosci* 27:3017–3029.
- Reyes A, Lujan R, Rozov A, Burnashev N, Somogyi P, Sakmann B (1998) Target-cell-specific facilitation and depression in neocortical circuits. *Nat Neurosci* 1:279–285.
- Rizo J (2018) Mechanism of neurotransmitter release coming into focus. *Protein Sci* 27:1364–1391.
- Rollenhagen A, Satzler K, Rodriguez EP, Jonas P, Frotscher M, Lubke JH (2007) Structural determinants of transmission at large hippocampal mossy fiber synapses. *J Neurosci* 27:10434–10444.
- Rozov A, Burnashev N, Sakmann B, Neher E (2001) Transmitter release modulation by intracellular Ca<sup>2+</sup> buffers in facilitating and depressing nerve terminals of pyramidal cells in layer 2/3 of the rat neocortex indicates a target cell-specific difference in presynaptic calcium dynamics. *J Physiol* 531:807–826.
- Salin PA, Scanziani M, Malenka RC, Nicoll RA (1996) Distinct short-term plasticity at two excitatory synapses in the hippocampus. *Proc Natl Acad Sci U S A* 93:13304–13309.
- Scanziani M, Gahwiler BH, Charpak S (1998) Target cell-specific modulation of transmitter release at terminals from a single axon. *Proc Natl Acad Sci U S A* 95:12004–12009.
- Seese RR, Wang K, Yao YQ, Lynch G, Gall CM (2014) Spaced training rescues memory and ERK1/2 signaling in fragile X syndrome model mice. *Proc Natl Acad Sci U S A* 111:16907–16912.
- Silinsky EM, Searl TJ (2003) Phorbol esters and neurotransmitter release: more than just protein kinase C? *Br J Pharmacol* 138:1191–1201.
- Sun HY, Lyons SA, Dobrunz LE (2005) Mechanisms of target-cell specific short-term plasticity at Schaffer collateral synapses onto interneurons versus pyramidal cells in juvenile rats. *J Physiol* 568:815–840.
- Tamamaki N, Nojyo Y (1993) Projection of the entorhinal layer II neurons in the rat as revealed by intracellular pressure-injection of neurobiotin. *Hippocampus* 3:471–480.
- Toth K, Soares G, Lawrence JJ, Philips-Tansey E, McBain CJ (2000) Differential mechanisms of transmission at three types of mossy fiber synapse. *J Neurosci* 20:8279–8289.
- Trieu BH, Kramar EA, Cox CD, Jia Y, Wang W, Gall CM, Lynch G (2015) Pronounced differences in signal processing and synaptic plasticity between piriform-hippocampal network stages: a prominent role for adenosine. *J Physiol* 593:2889–2907.
- Wang W, et al. (2016) A primary cortical input to hippocampus expresses a pathway-specific and endocannabinoid-dependent form of long-term potentiation. *eNeuro* 3.
- Wang W, Cox BM, Jia Y, Le AA, Cox CD, Jung KM, Hou B, Piomelli D, Gall CM, Lynch G (2018a) Treating a novel plasticity defect rescues episodic memory in fragile X model mice. *Mol Psychiatry* 23:1798–1806.
- Wang W, Jia Y, Pham DT, Palmer LC, Jung KM, Cox CD, Rumbaugh G, Piomelli D, Gall CM, Lynch G (2018b) Atypical endocannabinoid signaling initiates a new form of memory-related plasticity at a cortical input to hippocampus. *Cereb Cortex* 28:2253–2266.
- Weingarten DJ, Shrestha A, Juda-Nelson K, Kisiwaa SA, Spruston E, Jackman SL (2022) Fast resupply of synaptic vesicles requires synaptotagmin-3. *Nature* 611:320–325.
- Wiesner S, Legate KR, Fassler R (2005) Integrin–actin interactions. *Cell Mol Life Sci* 62:1081–1099.
- Witter MP (1993) Organization of the entorhinal–hippocampal system: a review of current anatomical data. *Hippocampus* 3:33–44.
- Witter MP (2007) Intrinsic and extrinsic wiring of CA3: indications for connective heterogeneity. *Learn Mem* 14:705–713.
- Witter MP, Doan TP, Jacobsen B, Nilssen ES, Ohara S (2017) Architecture of the entorhinal cortex a review of entorhinal anatomy in rodents with some comparative notes. *Front Syst Neurosci* 11:46.